The University of Adelaide

Department of Physics and Mathematical Physics

Differential Absorption Lidar for water vapour in the atmosphere

By

Kwang-Ho Bae

B.Sc.(Korea), B.Sc.(Hons.)(Adel.)

Thesis submitted for the degree of

Master of Science

In

July, 2002

Statement

This work contains no materials which has been accepted for the award of any other degree or diploma in any university or any other tertiary institution and, to the best of my knowledge and belief, contains no material previously published or written by another person, except where due reference has been made in the text.

I give consent to this copy of my thesis, when deposited in the University Library, being available for loan and photocopying.

Signed :

Date: 15/11/02

Acknowledgements

First of all, I would like to thank my supervisors, Dr. Murray W. Hamilton and Prof. R. A. Vincent, for their help and patience throughout my study. I would like to thank our department workshop staffs, Blair Middlemiss, Trevor Waterhouse and Graham Eames and all members of the Optics group. Also I would like to thank Frank Mayer, Prof. Volker Wulfmeyer and Dr. Martin Ostermeyer for their hospitality and useful discussions during my visit to University of Hohenheim, Germany.

Last, but not least, I wish to thank my parents, Jae-Seong Bae and Young-Hee Lee, my sister, In-Sook Bae, and my wife, Dong-Sook Kim, for their support during my study.

Contents

List of Figures

Chapter 1

Introduction

The atmosphere is mostly composed of nitrogen and oxygen. Nitrogen comprises about 78% and oxygen around 21% in dry air. The other 1% of the atmosphere comprises the other gases like argon (Ar), carbon dioxide, and ozone. However, the atmosphere around us is not completely dry. The atmosphere typically contains the small amount of water vapour and the distribution of water vapour depends on the temperature and height from the ground. This small amount of water vapour in the atmosphere affects greatly the weather of our planet on a global and local scale.

Water can change its phase from water vapour (gas) to water (liquid) or from water to water vapour. If water changes its phase to water vapour, some amount of heat should be absorbed by the water for its phase change. Of course when water vapour is changed into water, a certain amount of heat is emitted. This kind of heat exchange between water and the atmosphere has important effects on the weather and climate of the earth. In addition, a few percent change of humidity can affect the spectrum of outgoing long-wavelength radiation from the earth, and the effect of the water vapour is about twice as strong as that of carbon dioxide.[2,3] That is why water vapour is one of the major greenhouse gases with carbon dioxide and ozone. In addition, water vapour is a factor which determines the refractive index of air. The refractive index of air affects how far and wide radiowaves can travel in the atmosphere. The temporal and spatial information about the global and local distribution of water vapour is still insufficient. Some reasons are:

- The dynamic range of specific humidity varies with height over four orders of magnitude. The largest value of specific humidity is about 20 g/kg near the surface of the earth and the lowest value is about 0.001 g/kg near or above the tropopause that is the boundary between troposphere and stratosphere.

- There are sharp vertical gradients on scales of a kilometer or less and horizontal contrasts on scales of tens of kilometers in the distribution of water vapour in the atmosphere. The temporal variation is from minutes to decades, in the cases of convective process and climate change, respectively.

There are several methods to measure the distribution of water vapour in the atmosphere. First, balloon-born radiosondes with a hygrometer can measure the distribution of water vapour in the atmosphere. However, continuous measurement is impossible with this method because the balloon should be launched in the atmosphere by man, it takes several hours to take one measurement, and the radiosonde can be put in the atmosphere only two or three times a day.

Second, a ground-based Global Positioning System (GPS) uses the signal from satellites, and continuous measurement is possible with this method. However, we can not measure the vertical profile of water vapour with GPS.

Third, Differential Absorption Lidar (DIAL) transmits the pulses of laser into the atmosphere and receives the signal that is reflected by aerosols and water vapour in the atmosphere.[1] Continuous measurement of the distribution of water vapour in the atmosphere is possible with this LIDAR technique.

From the early 1970's, many DIAL systems have been developed [1,3-18] and recently many researchers have reported successful field tests.[14-17] Mostly, high power solid-state lasers, e.g. Ti:Sapphire and Alexandrite lasers, have been used as the transmitter of their DIAL systems. Although these DIAL systems operate well, the cost of development and maintenance is too high to install these systems in many places to investigate the effect of water vapour distribution over a more extensive range.[18] Therefore, we have been trying to develop a low cost and compact DIAL system for water vapour detection in the atmosphere.

The objective of our project is the development of Differential Absorption Lidar (DIAL) based on diode lasers for profiling the temporal and vertical distribution of water vapour in the atmosphere. DIAL is composed of transmitting and receiving parts. The transmitter of DIAL consists of two lasers. The wavelength of one laser must be tuned to the centre of water vapour absorption line and that of the other laser must be tuned to where water vapour does not absorb the laser beam. The master lasers of our DIAL are diode lasers around 830nm. The power of the master lasers will

need to be increased by means of an injection-locked master-slave design or a tapered amplifier when we want to observe water vapour in the higher atmosphere. The divergence of a laser beam should be small compared with the field of view of the receiving telescope. The receiving part of DIAL system consists of a telescope and a photodiode. In our DIAL system, a Schmitt-Cassegrain type telescope is used because the field of view of this telescope is big enough and the size of the telescope is reasonable. An avalanche photodiode (APD) will be used as the receiver of the light that is scattered by aerosols or water vapour in the atmosphere because its quantum efficiency is high and its response time is fast in the infrared region.

The objectives of this thesis are to apply frequency modulation spectroscopy to observe water vapour absorption lines in the infrared region and the wavelength locking of the master laser to the centre of water vapour absorption line. The root mean square (rms) deviation of the wavelength of the master laser from the centre of water vapour absorption line and the diameter of the transmitted beam in far field were measured. In addition, the receiving and transmitting telescopes were tested with a silicon photodiode.

The concept of DIAL is discussed in Chapter 2 and the relevant aspects of diode lasers and Fabry-Perot resonators are discussed in Chapter 3. In Chapter 4, the constructions of a confocal scanning Fabry-Perot and a multi-pass absorption cell are discussed. The temperature and current controllers of the master laser are discussed as well in this chapter. In Chapter 5, the concept of frequency modulation spectroscopy, including first and second harmonic detection, is discussed briefly. In Chapter 6, water vapour detection and measurement of absolute humidity by means of frequency modulation spectroscopy are discussed. The experiment to lock the wavelength of the master laser to the centre of water vapour absorption line is discussed there as well. In Chapter 7, the experiments to measure beam divergence in far field and to test the transmitting and receiving telescopes, using a silicon photodiode, are presented. Conclusions and future plans are discussed in Chapter 8. In addition, the diagram of a current-locking circuit is presented in Appendix A.

Chapter 2

DIfferential Absorption Lidar (DIAL)

Using Differential Absorption Lidar (DIAL), we can obtain two kinds of information on a target molecule. One is the concentration of the target in the atmosphere and the other is its distribution. The concept and types of LIDARs are discussed in section 2.1. The concept of Differential Absorption Lidar (DIAL) is discussed in session 2.2. Water vapour absorption lines around the infrared region from HITRAN (HIgh resolution TRANsmission molecular absorption) database[29] are presented in section 2.3. The design of our DIAL system is discussed in session 2.4.

2.1. Introduction

Differential Absorption Lidar (DIAL) is one of the remote sensing techniques. Generally speaking, there are two classes of the remote sensing techniques. One is 'passive remote sensing' and the other is 'active remote sensing'. The difference between the two techniques is whether an energy source is transmitted to the targets. Passive remote sensing does not use an energy source but receives the signal produced by the target, for example radiative emission. Conversely, active sensing uses radiowaves or the laser as an energy source.

RAdio Detection And Ranging (RADAR) uses radiowaves and receives some of the power that is scattered by aerosols or target molecules in the atmosphere. LIDAR operates like RADAR but LIDAR uses lasers as an energy source instead of radiowaves. The change in the properties of the scattered light enables some properties of the target molecule to be analysed. In addition, the time delay, between the light to travel toward the targets and that to be scattered back to the receiver of DIAL, is used to determine the range or height of the targets.

There are four basic types of LIDARs, which are 'Range-finder', 'Raman Lidar', 'Doppler LIDAR' and DIAL. A range-finder is the simplest LIDAR that is used to measure the distance to the targets. The pulses of a laser is transmitted to the targets and the time delay, between when the laser beam was transmitted and when the scattered light is received, is measured. Since we know the speed of light, the distance between the targets and the range-finder is simply the speed of light multiplied by the time delay. If several range-finders are located at different locations, then the position of the targets can be determined more accurately.

Raman Lidar uses the Raman scattering, by which the wavelength of the scattered light is shifted. Usually, narrow band filters are used to detect a particular wavelength of the scattered light. Using this Raman Lidar, mixing, scattering, or depolarization ratio of a molecule or molecules can be measured.

Doppler LIDAR uses the Doppler shift to measure velocity of the targets. The Doppler shift is the small change in wavelength due to the motion of the targets. The wavelength difference between the transmitted and received light can determine velocity of the targets. In other word, from the scattered light's intensity, polarization, wavelength, and linewidth, we can determine the range, refractive index, vibration spectrum, and velocity of the targets.

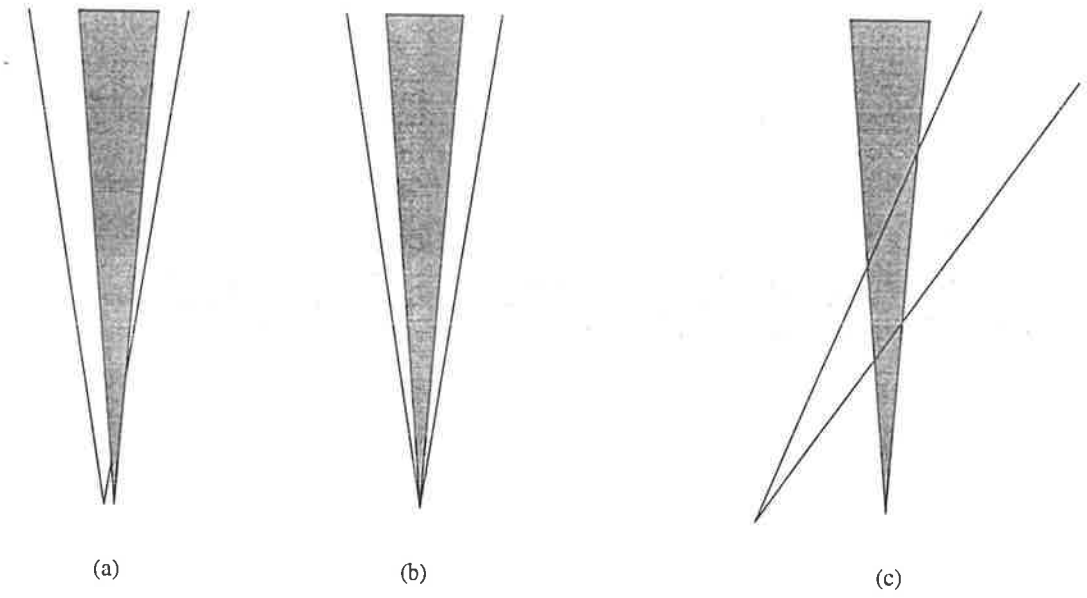

Figure 2.1 : Various types of LIDARs in terms of the location of a transmitter and a receiver. (a) : Mono-static and bi-axial; (b) : Mono-static and co-axial; (c) : Bi-static

LIDARs can be also classified as 'mono-static' and 'bi-static' according to the location of the transmitter and receiver of LIDAR as shown in Figure 2.1.[30] Mono-static LIDAR is a system which has its transmitter and receiver at the same location. It can be divided into two classes which are 'bi-axial' and 'co-axial'. In a co-axial system, the axis in which the laser beam is transmitted is the same as that of the receiver. In a bi-axial system, the axis in which light is transmitted is slightly different from that of the receiver. Bi-static LIDAR needs the maintenance of two locations: one is for the transmitter and the other is for the receiver. Mostly, mono-static LIDAR is preferred because the alignment of the transmitter and receiver is much easier. In addition, a co-axial system is preferred rather than a bi-axial system because the field of laser beam is exactly within the field of view of the receiver system, i.e. the field of view of the telescope of LIDAR.

Initially, water vapour Differential Absorption Lidars were made using temperature-tuned ruby lasers.[1,4,5] However, temperature drifts inside ruby could not give the long-term stability of the wavelength of the laser that is one of the essential requirement of the lasers for DIAL systems, and the optical efficiency of ruby was not good enough to achieve suitable laser power.

CO_2 lasers were used for measurement of water vapour distribution up to 2km altitude using direct detection [6,7] and as much as 6km using heterodyne detection.[8,9]

Dye lasers had been used for long-term stability of DIAL systems.[10-12] However, the high gain of dye lasers yielded low spectral purity which was caused by amplified spontaneous emission. In addition, the lifetime of the dye was relatively short compared with that of the other lasers.

Solid-state lasers like Alexandrite, Ti:Sapphire, and diode laser have replaced dye lasers. Alexandrite lasers could achieve sufficient frequency stability and narrow linewidth using a wavelength-selective medium inside the cavity.[12-15] However, wavelength drift of this wavelength-selective medium, which was caused by the change in the temperature of it, restricted the long-term stability of the laser system. In addition, hot spots in the cavity gave rise to optical damage of the laser rod and the other optical elements inside the resonator. Another approach to improve the long-term frequency stability of the alexandrite laser was an injection-locked master-slave design.[16] The master laser of this system was a cw Ti:Sapphire ring laser which was injected to the slave laser (a Q-switched linear alexandrite laser).

Wulfmeyer and Bösenberg in MPI (Max-Plank Institut für Meteorologie) reported a DIAL system using master-slave design lasers with 720nm wavelength and about 1 W power.[17] LASE (Lidar Atmospheric Sensing Experiment) of NASA in U.S.A., DLR (Deutsche Forschungsanstalt für Luft und Raumfahrt) in Germany and CNRS (Service d'Aèronomie du Centre National de la Recherche Scientifique) in France have used a master-slave design using an injection-seeded laser with around 720nm wavelength and about 1 W power of laser. Differential Absorption Lidar based on diode lasers is under construction at NOAA (National Oceanic and Atmospheric Administration) in U.S.A..[18] Most recently, ESA (European Space Agency) is developing a space-borne DIAL, WALES (WAter vapour Lidar Experiment in Space) using Ti:Sapphire lasers with 940nm wavelength.

2.2. Concept of DIfferential Absorption Lidar (DIAL)

Differential Absorption Lidar (DIAL) is used to measure the concentration of the target molecule as a function of range or height. The transmitter of DIAL consists of two lasers and their powers are the same. The on-line wavelength is exactly tuned to one of the absorption peaks of the target molecule. The off-line wavelength is shifted from the on-line wavelength and is where the power of the laser beam is not absorbed. The power of the scattered laser beam falls off as the distance (R) from the target increases according to the $\frac{1}{R^2}$ rule. The power of the scattered beam at the on-line wavelength will be equal or smaller than that of the scattered beam at the off-line wavelength depending on whether water vapour exists or not. From the power difference between the on-line and the off-line, we can obtain information on the water vapour concentration in the atmosphere. In addition, the time delay of the transmitted and scattered beam can give us the height of water vapour. Thus, the water vapour distribution as a function of height can be obtained.

Figure 2.2 is a schematic sketch of DIAL system. The laser beam is transmitted to the atmosphere and the vertical resolution depends on the length of the laser pulse. There is the time delay between the on-line and the off-line to distinguish the pulses. In the case of 500ns pulse, the vertical resolution is about 200m. As mentioned before, some

amount of the on-line beam's power is absorbed by water vapour and the power of the off-line is not. The scattered light is received by an optical receiver of DIAL system which consists of a telescope and a photodiode. In addition, a narrow bandwidth filter is needed to receive the scattered light whose wavelength is only around the on-line and the off-line wavelength.

Figure 2.3 is the expected data from the optical receiver of DIAL. The solid and dashed line represent the power of the on-line and the off-line, respectively. The number of photons (N_A) that is absorbed by water vapour in the region between R_1 and R_2 can be written as[1]

$$N_A = \frac{1}{2(R_1 - R_2)[\sigma(\lambda_{on}) - \sigma(\lambda_{off})]} \ln\left[\frac{P_{on}(R_1)\cdot P_{off}(R_2)}{P_{off}(R_1)\cdot P_{on}(R_2)}\right] \qquad (2\text{-}1)$$

where λ_{on} and λ_{off} are the on-line and the off-line wavelength, respectively, $\sigma(\lambda)$ is the cross-section of water vapour at λ, and P_{on} and P_{off} are the power of the scattered light of the on-line and the off-line, respectively.

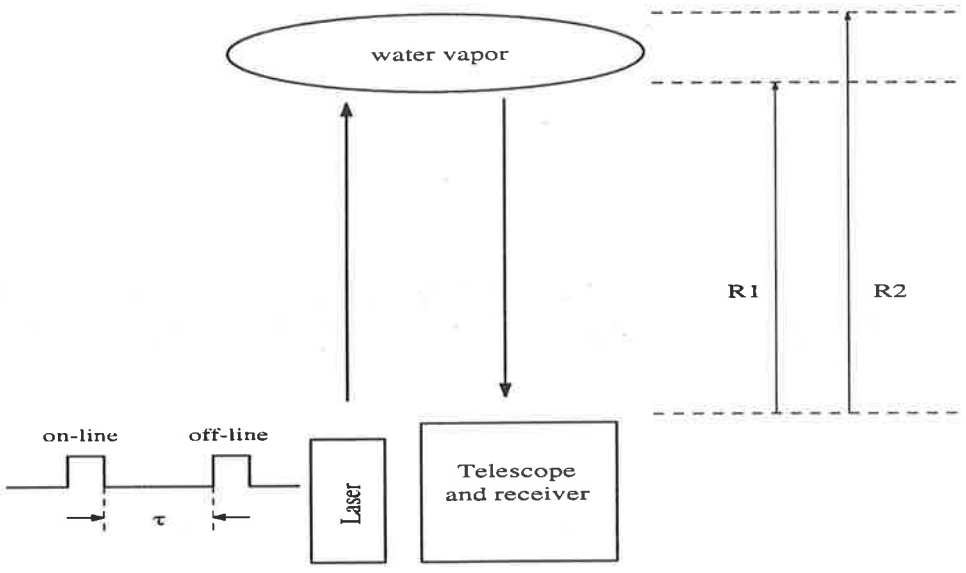

Figure 2.2 : Brief schematic of DIAL. τ is the time delay between on-line and off-line pulses and we can distinguish the two pulses using this time delay. Suppose that water vapour exists only in the region between R1 and R2.

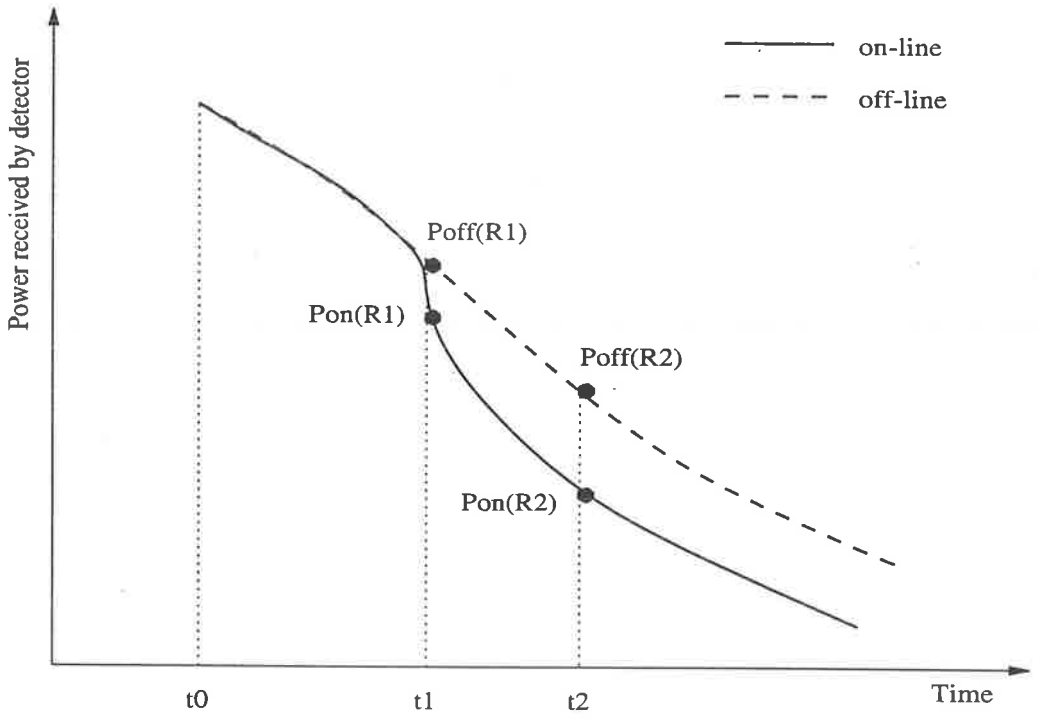

Figure 2.3 : Expected data of DIAL in situation like Figure 2.2. t_o is the time when we start receiving the scattered light. t_1 and t_2 represent height R_1 $(= c \cdot t_1)$ and R_2 $(= c \cdot t_2)$ in time domain where c is the speed of light.

2.3. Water vapour absorption lines from HITRAN database

The absorption lines of various molecules can be found in HITRAN (HIgh-resolution TRANmission molecular absorption) database[28,29] which is mostly theoretically calculated. The unit of intensity in HITRAN database is $cm^{-1}/(molecule \cdot cm^{-2})$ which had been chosen for the convenience of calculation. Figure 2.4 shows the water vapour absorption lines around the infrared region from 700nm to 950nm at 296K. Around 940nm and 830nm, there are many water vapour lines as shown in Figure 2.5 and Figure 2.6.

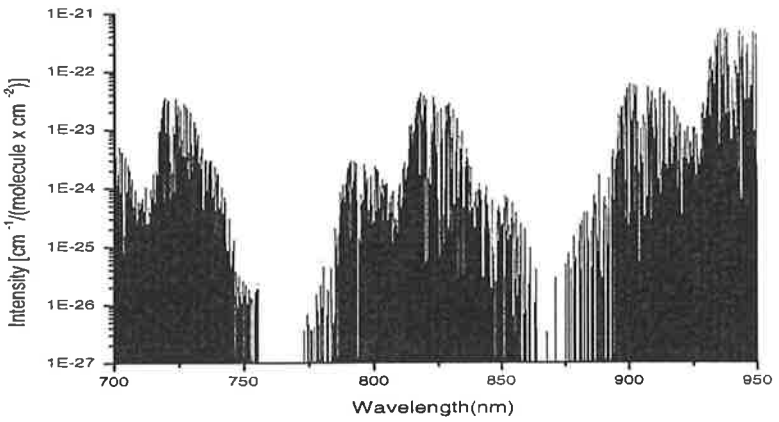

Figure 2.4: Water vapour absorption lines around the infrared region (from HITRAN).

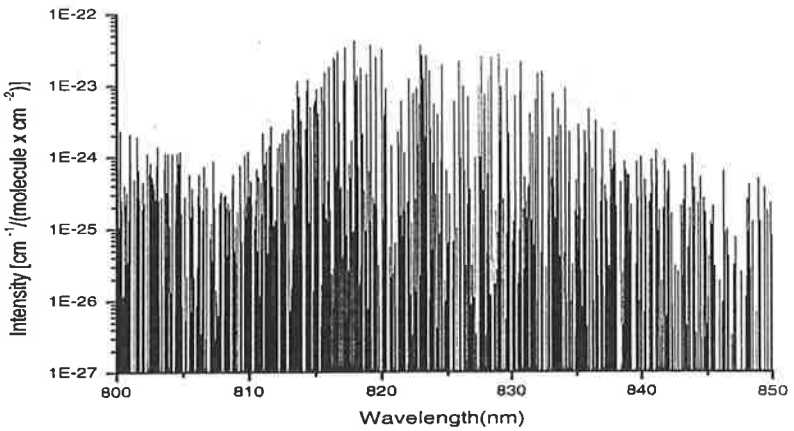

Figure 2.5 : Water vapour absorption lines from 800nm to 850nm (from HITRAN).

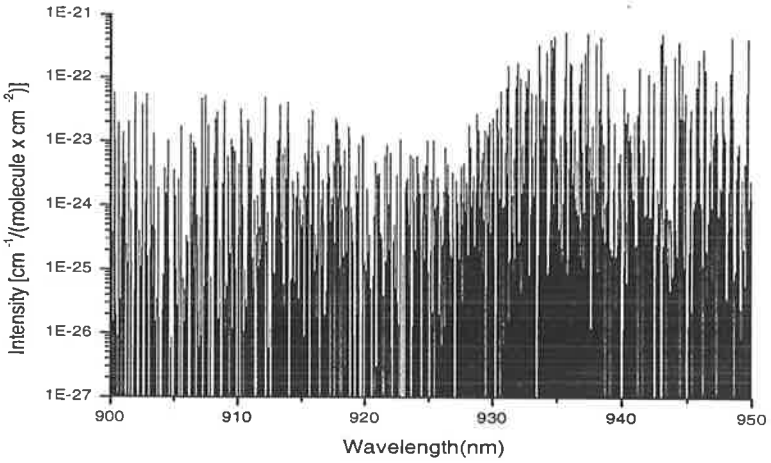

Figure 2.6 : Water vapour absorption lines from 900nm to 950nm (from HITRAN).

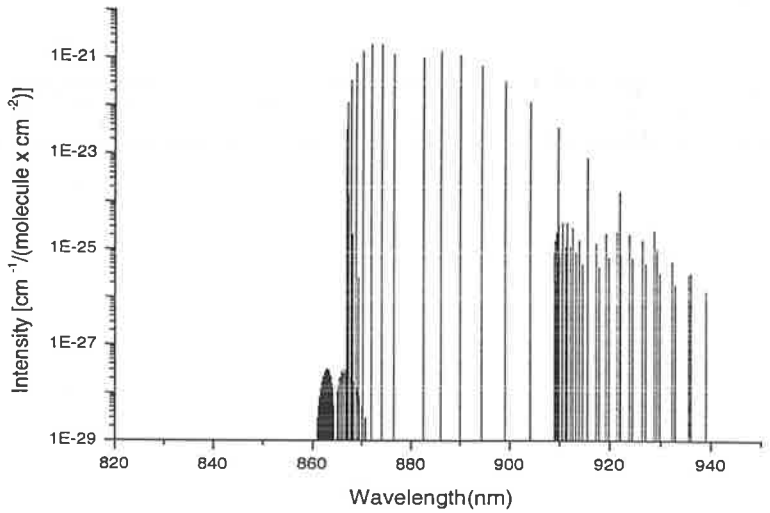

Figure 2.7 : The absorption lines of the other gases, 34 kinds of molecules included in HITRAN database except of water vapour(H_2O), from 850nm to 950nm (from HITRAN).

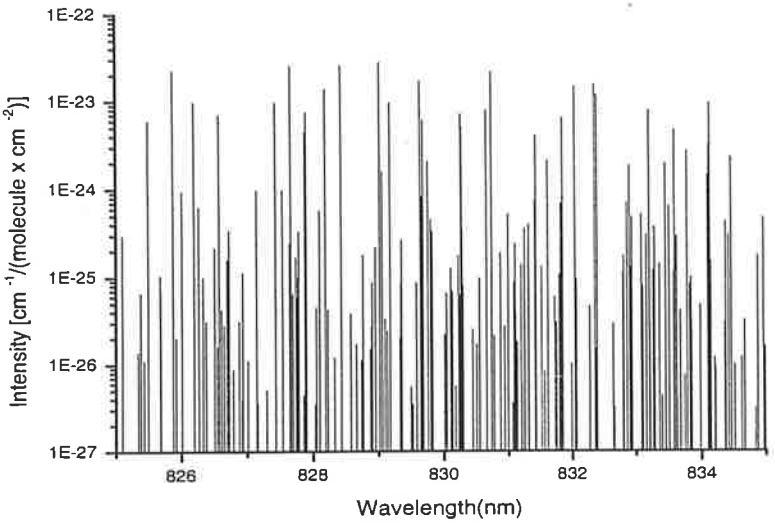

Figure 2.8 : Water vapour absorption lines around 830nm (from HITRAN).

The wavelength of the transmitter of our ground-based DIAL is around 830nm, although the strength of the absorption lines around 900nm is stronger. There are three reasons for this. First, there are several water vapour absorption lines, whose line strength is about 1×10^{-23} cm/molecule. This absorption line strength is appropriate for our DIAL system. Second, there is no absorption line of the other molecules like nitrogen, oxygen, or other gases according to HITRAN database as shown in Figure 2.7. Third, we found a low power diode laser (Hitachi HG8325G) which operates in a single longitudinal mode and has good beam quality and wide tuning range in this wavelength region.

2.4. Requirement of lasers for detecting water vapour in the atmosphere

Parameter	Requirement		Specification				
	Water	Temperature	MPI	CNRS	LaRC	LASE	DLR
Wavelength (nm)	720-730	767-771	720-780	720-780	727-733	812-819	720-725
Linewidth (MHz)	<400	<130	<40	<570	<280	<500	<450
Frequency stability (MHz)	±210	±75	15 rms	±180	±170	±210	±450
Spectral Purity (%)	>99.5	>99.9	>99.99	>99.99	>99	>99	>99
Pulse length (ns)	<200		<200	<250	<200	<30	<20
Divergence (mrad)	<1		0.4	n.s.	1.5	n.s.	0.5
Energy per pulse (mJ)	>50		>50	>50	>60	>150	>30
Repetition rate (Hz)	>10		>15	10 d.p.	10 d.p.	5 d.p.	10
$\Delta\nu_{on,off}$ (GHz)	<55		50	≈250	≈100	n.s.	≈225
Beam profile			TEM_{00}	mm	n.s.	mm	mm

Table 2.1: The requirement of a laser system for water vapour detection (with an overall error < 5 %) and temperature measurement (with an overall error < 1 K) and current operating DIAL systems. Errors that come from atmosphere effects were not taken account.; n.s.: not specified in the literature; d.p. : double-pulse operation; $\Delta\nu_{on,off}$: frequency difference between on and off line (on and off line is described in Chapter 3). The abbreviations of institutes stand for MPI (Max-Plank Institute für Meteorologie), CNRS (Service d'Aèronomie du Centre National de la Recherche Scientifique) in France, LaRC (NASA Langley Research Centre), LASE (Lidar Atmospheric Sensing Experiment) in U.S.A., and DLR (Deutsche Forschungsanstalt für Luft und Raumfahrt) in Germany, respectively (from Ref. 17).

Beam quality and wavelength stability of lasers are very important for the performance of Lidar. First of all, the longitudinal mode of the laser must be a single mode and the linewidth of the laser should be considerably smaller than the linewidth of the absorption line of water vapour. Because Full Width at Half Maximum (FWHM) of the absorption line of water vapour is order of 1 GHz, less than 400 MHz

linewidth of the laser is required. In addition, the wavelength of the laser must be tuned to the centre of the absorption line of water vapour. Hence, the rms frequency deviation from the centre of water vapour absorption line is very important as well. About $\pm$ 200 MHz of frequency stability is required for the detection of water vapour in the atmosphere and about $\pm$ 70 MHz is needed for measurement of temperature to reduce the errors of measurement.[17] In addition, a short pulse width of the laser beam is required because a smaller pulse width gives better vertical resolution. Spectral purity - the ratio of the pulse energy within a given linewidth to the overall pulse energy - must be reasonably small as well. For example, if spectral purity of the laser is 100 %, this means the whole energy of pulse is within a given linewidth. More than 99 % spectral purity of the laser is required usually. Table 2.1 is the requirement of the laser for water vapour detection (with an overall error < 5 %) and temperature measurement (with an overall error < 1 K) and specifications of current Differential Absorption Lidars around the world.

2.5. Design of our planned ground-based DIAL system

Figure 2.9 is a brief diagram of our planned ground-based DIAL system. There are two master lasers, which are diode lasers, and the wavelength of these lasers is around 830nm. The wavelength of the on-line master laser is tuned to one of the water vapour absorption lines around 830nm by means of a multi-pass absorption cell. The multi-pass absorption cell consists of two identical parabolic mirrors and some portion of the on-line master laser travels inside the cell. The path length inside the cell is about 24m and water vapour absorption lines are detected by frequency modulation spectroscopy. In addition, the frequency difference between on-line and off-line is about 10GHz. An Acousto-Optic Modulator (AOM) chops the beam of the master lasers and the length of the pulse is about 500ns. The laser beams of the master lasers are combined with the slave laser. The power of our transmitter is about 0.5 W and the sensitivity we expect is about 0.5 g/kg at 4km range.[18] The transmitting telescope of our system is a Schmitt-Cassegrain telescope and a narrow bandwidth filter is used after the transmitting telescope. An avalanche photodiode is used to detect the

scattered light by aerosols and water vapour in the atmosphere and a desktop computer is used to store data and to control the other optics and electronics.

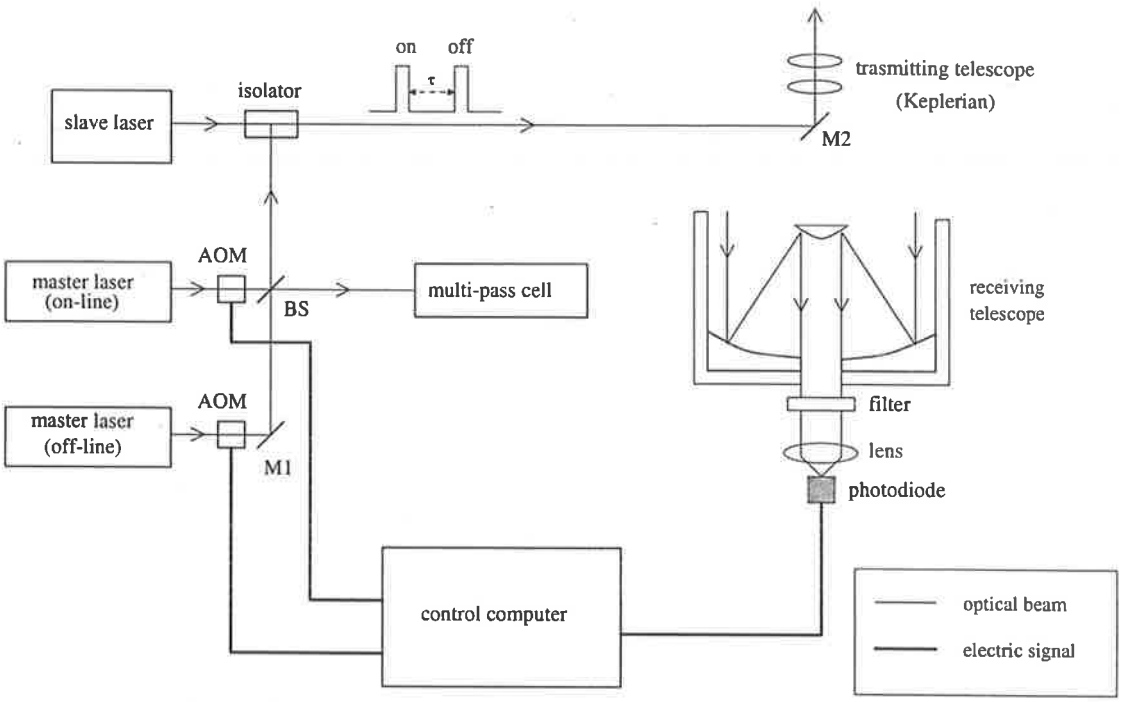

Figure 2.9 : Schematic diagram of our planned DIAL system. M : mirrors; AOM : Acousto-Optic Modulator. τ is the time delay between the on-line and the off-line pulses and we can distinguish the two pulses using this time delay.

Chapter 3

Basics of diode lasers

Diode lasers have been used in many fields of laser applications, e.g. laser printer, laser spectroscopy, pump source for high power lasers, and so on. The basic theory of operation is similar as a forward-bias diode and much complicated structures have been developed to produce greater power or to meet specific needs. In terms of laser spectroscopy, a diode laser is very important because it has wide range of wavelength, compact size, good laser modal quality, and reasonable power. After the invention of diode lasers, many laser spectroscopy researchers have used diode lasers for these reasons.

In section 3.1, the relevant aspects of diode lasers are discussed. In section 3.2, the resonance modes of Fabry-Perot resonators are discussed because a confocal scanning Fabry-Perot was used in water vapour spectroscopy in order to investigate the quality of scanning and to obtain the frequency difference between the observed water vapour absorption lines.

3.1. Diode lasers

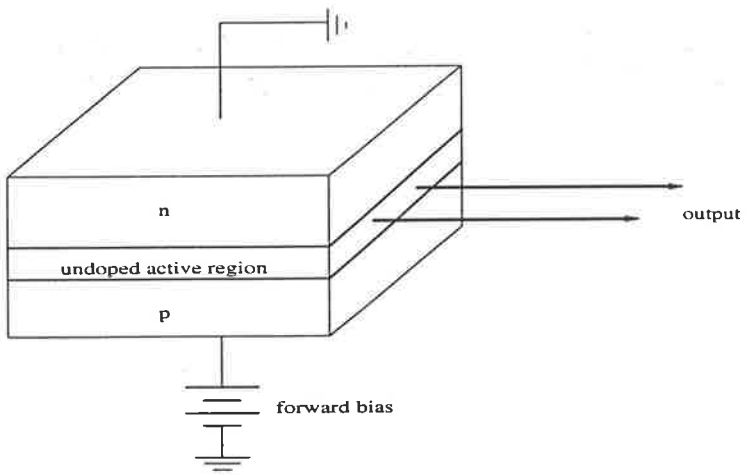

Figure 3.1 : Typical structure of a diode laser

A semiconductor material is used as a gain medium in diode lasers. Most of semiconductor materials are fabricated from III-V compounds which is formed by elements from third to fifth column of the periodic table. $Al_{1-x}Ga_xAs$ and $In_{1-x}Ga_xAs_{1-y}P_y$ are the most common semiconductor materials for diode lasers. Parameters, x and y, change from 0 to 1 and thus, $Al_{1-x}Ga_xAs$ can represent from AlAs (x=0) and GaAs(x=1). The wavelength range of $Al_{1-x}Ga_xAs$ is around from 780nm to 880nm and that of $In_{1-x}Ga_xAs_{1-y}P_y$ is approximately from 1150nm to 1650nm. Figure 3.1 is a typical structure of a diode laser, i.e. n-type, p-type semiconductors and an undoped active region. An undoped active region is usually called 'p-n junction' and laser beam is emitted from the p-n junction, if a sufficient amount of forward-bias is supplied.

The intensity profile of the output beam – i.e. transverse mode – mainly depends on the thickness and the structure of the p-n junction, the refractive index difference between the junction and n-type or p-type semiconductor. In addition, the output power of diode lasers depends on the current and temperaure of the diode lasers. Below threshold, a diode laser acts like a LED (Light Emitting Diode) producing a small amount of incoherent light. Conversely, above threshold, a diode laser starts emitting coherent light. If the current is above the 'damage threshold', the diode laser can be damaged, sometimes permanently. That is why the design of a current-controlled power supplier is important.

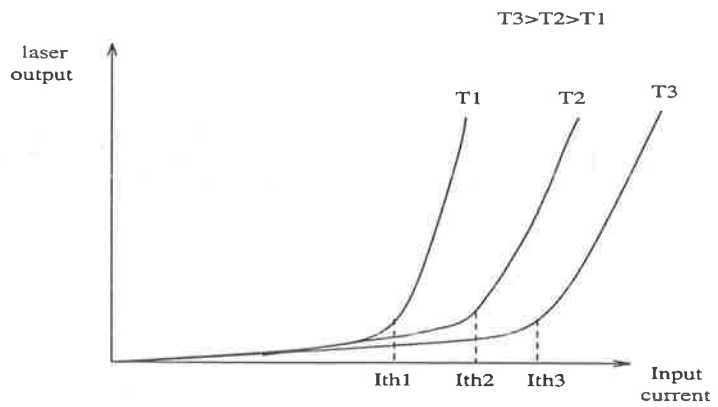

Figure 3.2 : Schematic sketch of the output of a diode laser as a function of input current in three different operating temperature. T1, T2, and T3 are different temperature of diode laser. Ith1, Ith2, and Ith3 represent threshold currents in cases of T1, T2, and T3, respectively.

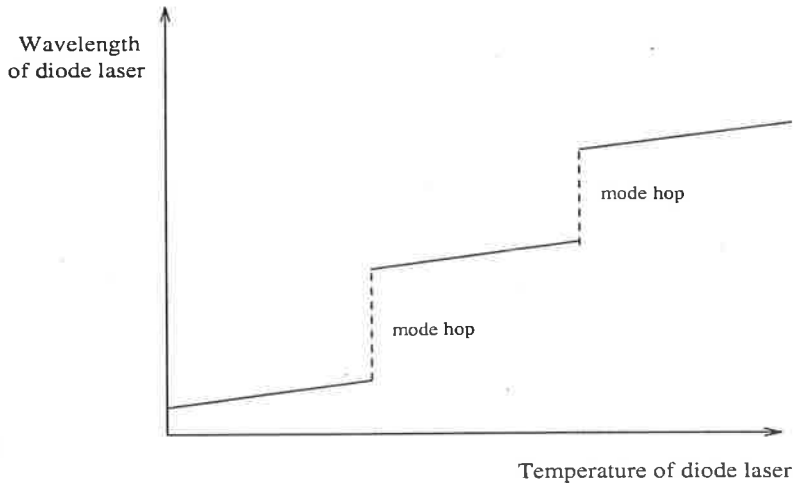

Figure 3.3 : Schematic of 'mode hop' of a diode laser

As shown in Figure 3.2, the output power of a diode laser depends on the temperature of the diode laser. Also, the threshold current of it increases as the temperature of the diode laser does. In addition, the wavelength of the diode laser depends on both current and temperature. Therefore, we can scan the wavelength of the diode lasers by scanning the temperature or current of the diode lasers. This method will be discussed in Chapter 5 and Chapter 6.

Ideally, above the threshold current, the wavelength of a diode laser should depend linearily on temperature. However, in reality, there are many discontinuities as shown in Figure 3.3 and these discontinuities in the wavelength of laser are called 'mode-hops'. Therefore, we usually can not continuously scan the wavelength of a diode laser. However, we found a diode laser (Hitachi HG8325G) and the mode-hop free scanning range of this diode laser was several hundred GHz while operating in a single longitudinal mode.

The output of a diode laser typically has an elliptical intensity profile as shown in Figure 3.4. In the direction perpendicular to the junction – xz plane in Figure 3.4 –, the beam is confined by the narrow p-n junction. Therefore, the beam is spread in this direction for diffraction and the diffraction angle is as large as several tens of degrees. That is why the divergence angle in xz plane, θ_{xz}, is typically bigger than that in xy plane, θ_{xy}.[24] This problem may be corrected, at least partially, by the use of a collimating lens.

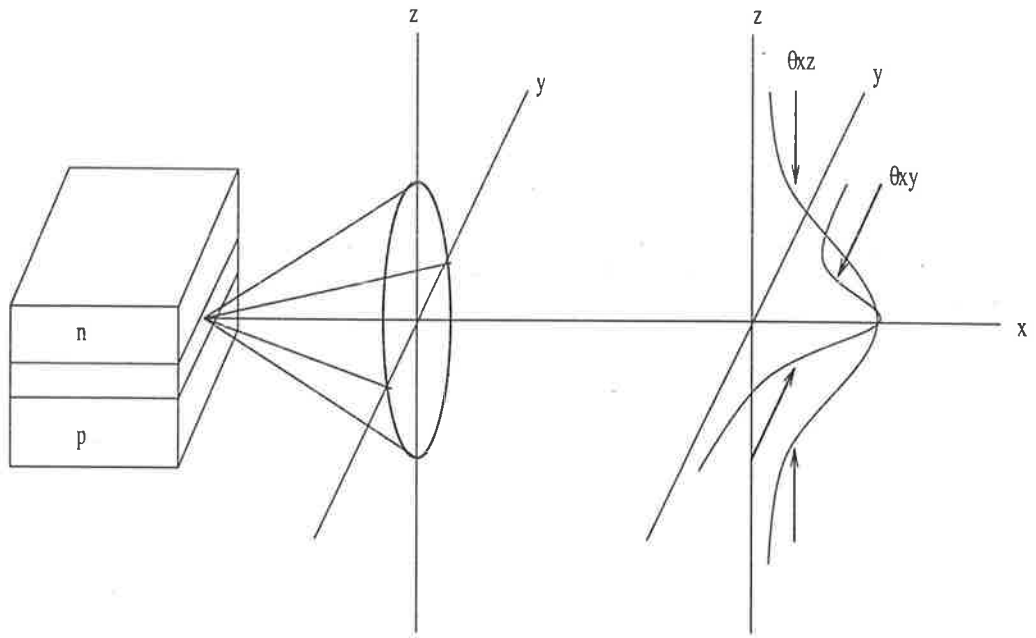

Figure 3.4 : Schematic of the divergence of the output of a diode laser

3.2. Fabry–Perot resonators

In this section, the resonance modes of Fabry-Perot resonators will be discussed and the details can be found in Ref. 20, 25, 26 and 27. We have used a confocal scanning Fabry-Perot for these three reasons. First, it is needed to make it sure that the master laser is operating in a single longitudinal mode. Second, when the laser is scanned and modulated, the smoothness of scanning or modulating can be monitored using this scanning Fabry-Perot. Third, using Free Spectral Range (FSR) of Fabry-Perot, the frequency difference between the observed water vapour absorption lines can be found and, in addition, we can find the wavelength of those absorption lines compared with HITRAN database.

Consider the resonance condition of resonators in longitudinal or 'axial' direction. It can be written as

$$kd = q\pi \tag{3-1}$$

or

$$\upsilon = \frac{c}{2nd} q \tag{3-2}$$

where k is the wavenumber, q is the integer that represents a longitudinal mode of a resonator, d is the length of a resonator, υ is the frequency of laser beam, n is the refractive index inside a resonator, and c is the speed of light. Thus, the wavenumber difference between two adjacent longitudinal modes, $\Delta k'$, can be written as

$$\Delta k' = k_{q+1} - k_q = \frac{\pi}{d}. \tag{3-3}$$

In addition, the frequency difference between two adjacent longitudinal modes, $\Delta\upsilon'$, can be expressed as

$$\Delta\upsilon' = \upsilon_{q+1} - \upsilon_q = \frac{c}{2nd}. \tag{3-4}$$

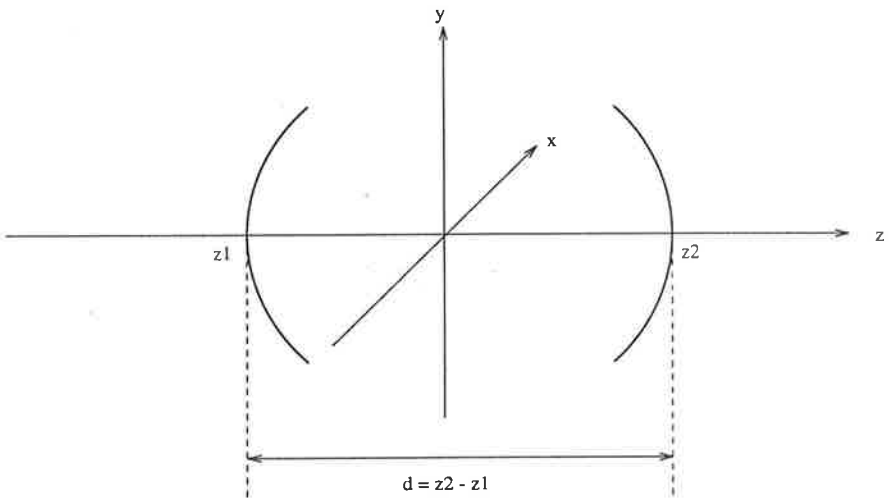

Figure 3.5 : A spherical resonator consisting of two identical spherical mirrors which are located at z_1 and z_2. The length of the resonator, d, is $|z_2 - z_1|$.

Now, we discuss the resonance condition of a resonator in transverse directions, which are perpendicular to axial direction, i.e. x and y in Figure 3.5. Consider a resonator consisting of two identical spherical mirrors. In this case, the resonance conditon for a transverse mode, m and p, can be written as

$$\theta_{mp}(z_2) - \theta_{mp}(z_1) = q\pi \tag{3-5}$$

where $\theta_{mp}(z)$ is the phase shift of the laser beam at z. $\theta_{mp}(z)$ can be expressed

$$\theta_{mp}(z) = kz - (1+m+p)\tan^{-1}\left(\frac{z}{z_0}\right), \tag{3-6}$$

$$z_0 = \frac{\pi\omega_0^{\,2} n}{\lambda} \tag{3-7}$$

where λ is the wavelength of the laser beam and ω_0 is the beam waist. Therefore, the resonance condition of the resonator for a laser mode, *m, p* and *q*, can be expressed

$$k_q z - (1+m+p)\left[\tan^{-1}\left(\frac{z_2}{z_0}\right) - \tan^{-1}\left(\frac{z_1}{z_0}\right)\right] = q\pi. \tag{3-8}$$

In the case of fixed m and p, the resonance condition can be

$$\Delta k = k_{q+1} - k_q = \frac{\pi}{d}, \tag{3-9}$$

which is the same as Eq. (3-3) and the frequency difference, $\Delta\upsilon$, can be expressed

$$\Delta\upsilon = \frac{c}{2nd}\Delta(m+p). \tag{3-10}$$

In the case of fixed q, the resonace condition can be written as

$$(k_1 - k_2)d = [(1+m+p)_1 - (1+m+p)_2]\left[\tan^{-1}\left(\frac{z_2}{z_0}\right) - \tan^{-1}\left(\frac{z_1}{z_0}\right)\right], \tag{3-11}$$

and

$$\Delta\upsilon = \frac{c}{2\pi nd}\Delta(m+p)\left[\tan^{-1}\left(\frac{z_2}{z_0}\right) - \tan^{-1}\left(\frac{z_1}{z_0}\right)\right] \tag{3-12}$$

where subscript 1 and 2 represent two different laser modes and $\Delta(m+p)$ is the difference between the additions of two different transverse modes, *m* and *p*.

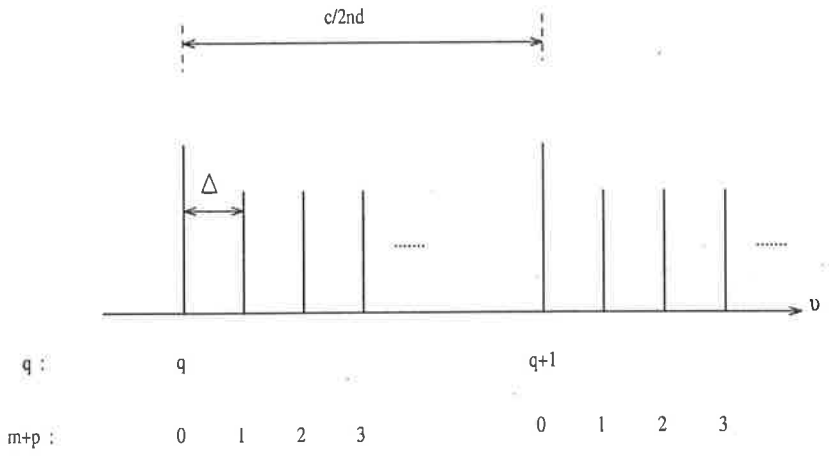

Figure 3.6 : Positions of the resonance frequencies of a non-confocal resonator (R>d) as a function of the mode indices and $\Delta = \frac{c}{2\pi n z_0}$.

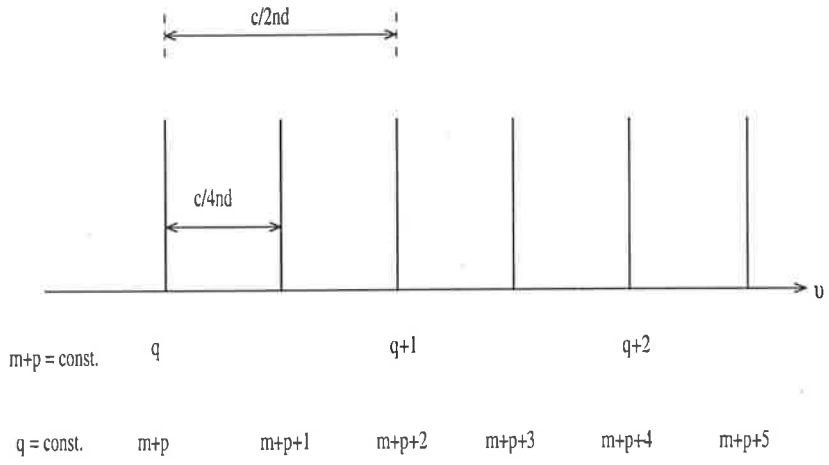

Figure 3.7 : Positions of the resonance frequencies of a confocal resonator (R=d) as a function of the mode indices – m, p , and q.

In the case of $R > d$, $|z_1|$ and z_2 is much smaller than z_0, thus $\tan^{-1}\left(\frac{z_1}{z_0}\right) \approx \frac{z_1}{z_0}$.

Therefore, the resonance condition for this case can be written

$$\Delta\upsilon \approx \frac{c}{2\pi nd}\Delta(m+p)\left[\frac{z_2}{z_0} - \frac{z_1}{z_0}\right]$$

$$= \frac{c}{2\pi nd}\Delta(m+p)\frac{d}{z_0} \qquad (3\text{-}13)$$

$$= \frac{c}{2\pi n z_0}\Delta(m+p).$$

The space between resonance modes is not regular as shown in Figure 3.6.

When the radius of mirrors, R, is the same as the length of a resonator, this resonator is called a confocal scanning Fabry-Perot which was used to investigate the modes of the master laser. In this case, $z_2 = z_0$ and $z_1 = -z_0$, the frequency difference, $\Delta\upsilon$, can be written

$$\Delta\upsilon = \frac{c}{4nd}\Delta(m+p). \tag{3-14}$$

The positions of the resonance frequencies of a confocal Fabry-Perot is shown in Figure 3.7 and the space between the resonance modes is regular. Therefore, a confocal scanning Fabry-Perot is better to investigate the spectral profile of unknown signal or laser beam. Usually $\Delta\upsilon$, which is in Eq. (3-14), is called Free Spectral Range (FSR) and Free Spectral Range must be bigger than the width of the spectral region that is investigated.

Chapter 4

Experiment |

Other optics and master lasers

This chapter is about the master laser and the other optics including a confocal scanning Fabry-Perot, a single mode optical fibre, and a multi-pass absorption cell. In section 4.1, the design of a confocal scanning Fabry-Perot and the mode of the master laser are discussed. In section 4.2 and 4.3, temperature and current controllers for the master laser of our DIAL system and schematic of the external port of these controllers to scan and modulate the wavelength of the laser are discussed. The design of the multi-pass absorption cell, by which the optical path length of laser beam can be increased, is discussed in section 4.4.

4.1. Construction of a confocal scanning Fabry-Perot

4.1.1. Design

Our confocal scanning Fabry-Perot consists of two identical concave mirrors (CVI PR2-830-98-0537-0.010CC), Piezo (Piezomechnik HPSt 150/20), metal housing, and a photodiode (RS 194-076). The centre wavelength of reflection of the mirrors is 830 nm, reflectance is 98 % at the centre wavelength, and the radius is 1 cm. The Piezo of our Fabry-Perot has a multi-layer structure and thus, we do not need to use hundreds of voltage as a conventional single layer Piezo. Therefore, a low voltage function generator (HAMEG HM8030) is used. Figure 4.1 is the brief schematic of the confocal scanning Fabry-Perot.

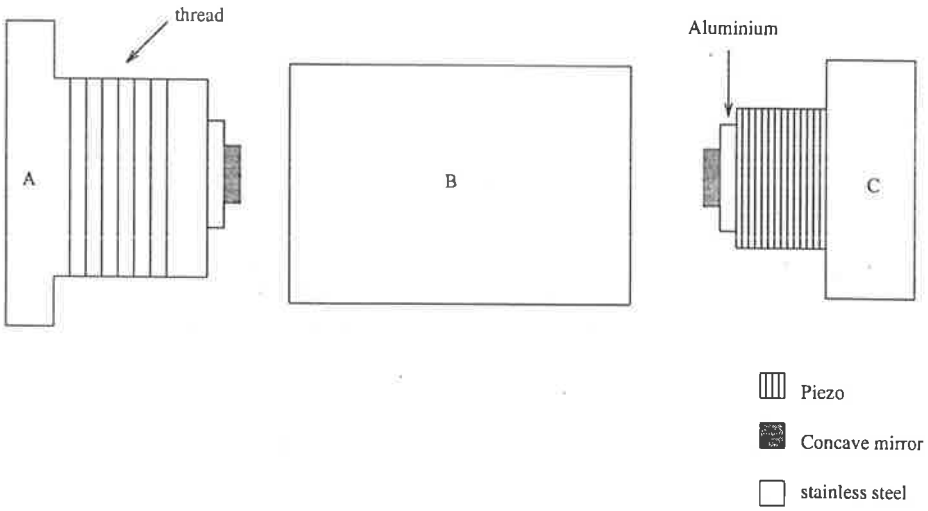

Figure 4.1 : Brief diagram of the confocal scanning Fabry-Perot

A concave mirror is mounted on mount (A) and the other mirror is mounted on the Piezo that is attached to mount (C). There are threads on each side of (A) and (B), i.e. the outside of (A) and the inside of (B). These threads make it possible to adjust the distance between the mirrors. Epoxy resin and hardener (RS 850-940) are used to bond the mirrors and the mounts. Two wires from the Piezo are connected to a SMB connector that is mounted on the surface of mount (C).

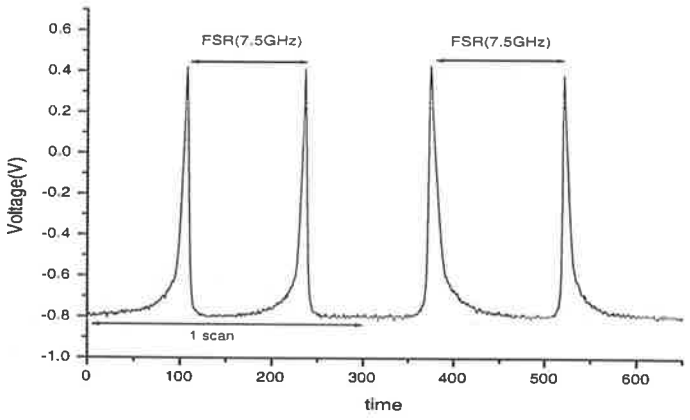

Figure 4.2 : Spectral profile of the master laser

Free Spectral Range (FSR) of the confocal scanning Fabry-Perot is 7.5 GHz by Eq. (3-14) assuming the refractive index is 1. Figure 4.2 is the spectral profile of the master laser (Hitachi HG8325G) measured by this confocal scanning Fabry-Perot.

Finesse (F) of this Fabry-Perot was measured as $F = \frac{FSR}{FWHM} \cong 75$ where $FWHM$ is the Full Width at Half Maximum of a peak. [25]

4.2. Temperature controller of diode lasers

4.2.1. Schematics

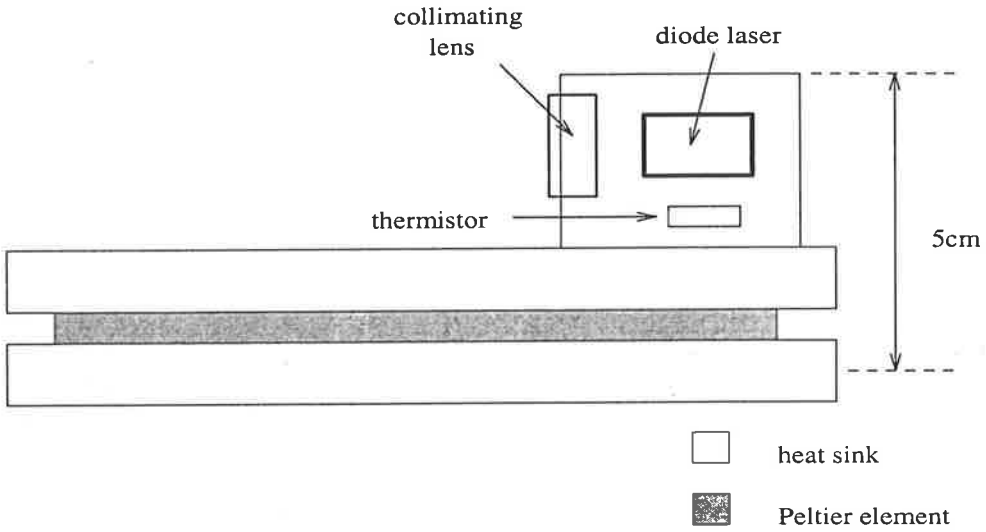

Figure 4.3 : Diagram of the master laser's mount

The temperature of the master laser is adjusted by a Peltier element or a thermoelectric cooler (TEC). As shown in Figure 4.3, the Peltier element is placed between two heat sinks. Another heat sink is for holding a diode laser and a collimating lens. A thermistor (5kΩ) is placed in the side of this heat sink and close to the diode laser. There is a precision temperature sensor (National Semiconductor, LM335) which is not shown in Figure 4.3 in order to measure the temperature of the diode laser.

The internal set-point of the temperature controller consists of the Wheatstone bridge as shown in Figure 4.4. In this case, the balance condition of this Wheatstone bridge can be expressed as

$$\frac{5}{(5-x)+5} = \frac{5+R_{therm}}{x} \tag{4-1}$$

where x is the value of resistance that is determined by the adjustment dial of 5kΩ potentiometer, i.e. the internal set-point of the temperature controller, and R_{therm} is resistance of the thermistor. The voltage difference across the Wheatstone bridge is amplified first and the output of this amplifier is called the error signal. Subsequent amplifications are carried out in parallel by proportional and integrating amplifiers. The details about the roles of proportional and integrating amplifiers in temperature controllers can be found in Ref. 33. These signals are added by a summing amplifier and sent to the Peltier element.

If the error signal is zero, then it means that the temperature of the diode laser is exactly what we want. If the error signal is not zero, then the temperature controller provides heating or cooling to the diode laser.

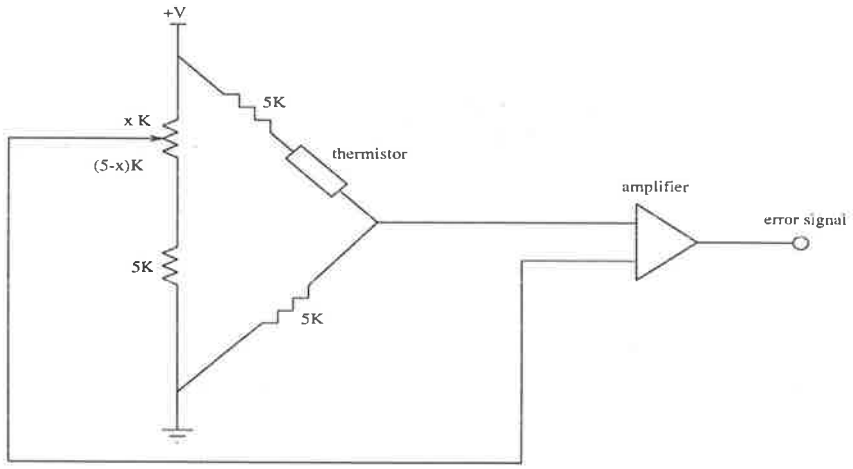

Figure 4.4 : The internal set-point of the temperature controller

4.2.2. External set-point

When frequency modulation spectroscopy is carried out, the temperature and current of the diode laser should be scanned or modulated at the same time or independently as mentioned before. Therefore, an external set-point of a temperature controller is needed. The external set-point can be made by modifying the Wheatstone bridge of the temperature controller as shown in Figure 4.5.

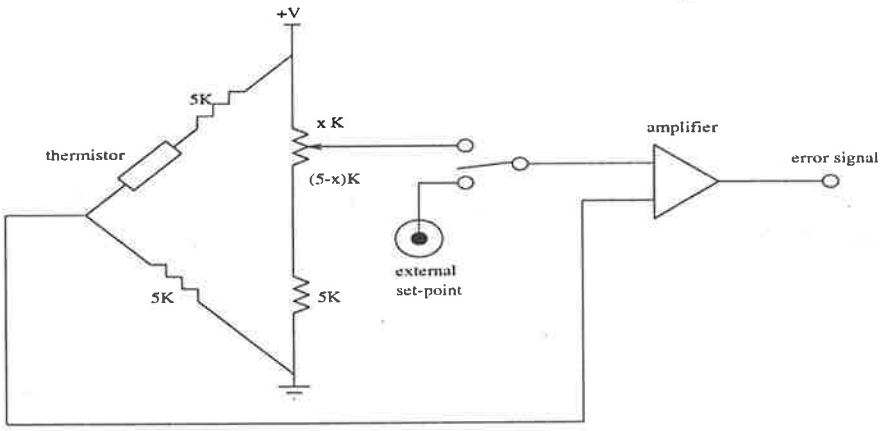

Figure 4.5: The external set point of the temperature controller

In addition, we should know the relation between 'external set-point voltage' and actual temperature. This information is crucial as we scan the diode laser using the external set-point of the temperature controller. The relation between them was measured as Table 4.2. A function generator (Wavetek model 64), producing various waveforms as slow as 0.001Hz, was used to scan the wavelength of the diode laser using the external port of the temperature controller.

Voltage (V)	Temperature (K)
2.5	283.7
3.0	289.1
3.5	296.6
4.0	305.3
4.5	318.0

Table 4.2: The relation between the voltages of the external set-point and temperature

4.3. Current controller of diode lasers

The current to a diode laser must be regulated and have low noise. In most case, better than 0.5mA of stability is needed. The voltage of the current supplier of the diode laser is in the range of 1 to 2 volt and thus, it can be powered by low voltage batteries. In addition, the optical power of the diode laser can be monitored by a photodiode beside the diode laser and the maximum optical power of the diode laser can be set as well.

4.3.1 Schematics and external modulation port

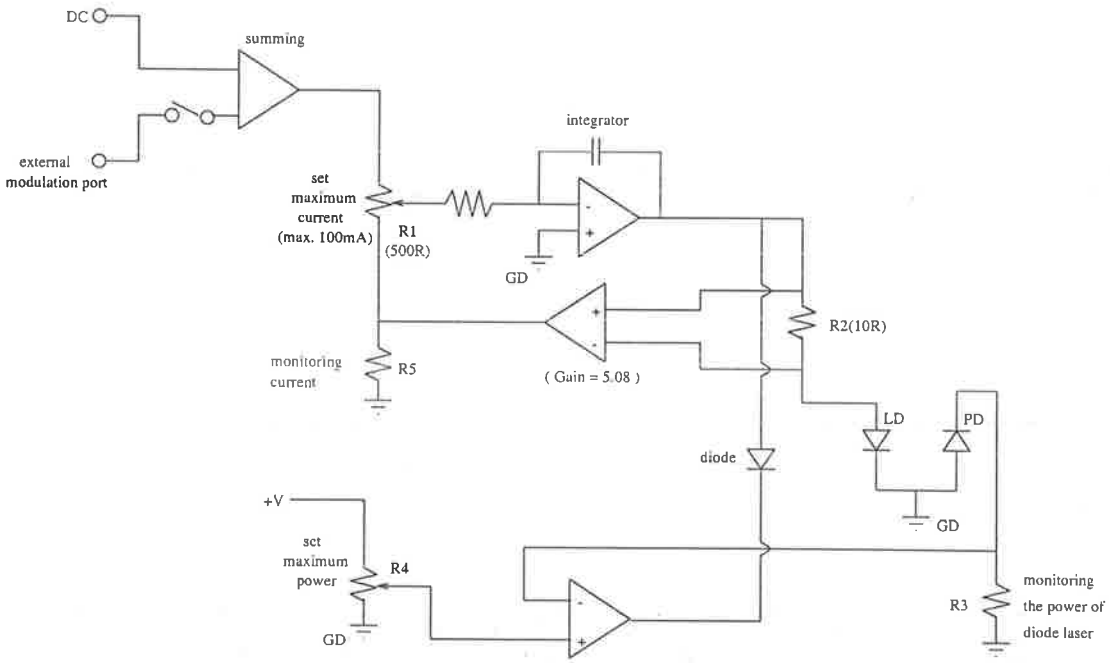

Figure 4.6 : Brief schematic of the current controller for the diode laser. R: resistor; GD: ground; LD: diode laser; PD: photodiode.

DC voltage and the signal from the external modulation port, which can be turn on and off by a switch, are added by a summing amplifier. The output of this amplifier is integrated in order to supply stable current to the diode laser. An additional features of our current controller is that we can monitor the optical power of the diode laser. If it

is greater than a certain value, then the current supplier is shut down automatically using the signal from the photodiode beside the diode laser and the maximum power set-point that is a variable resistor (R4) in Figure 4.6. In addition, using an external modulation port, the frequency of the diode laser can be modulated in the range of the order of hundred MHz.

4.4. Construction of a multi-pass absorption cell

A multi-pass absorption cell gives a longer path length to laser beam inside the cell and a version of that was presented by Herriot.[35] This configuration has found many applications in laser spectroscopy, gas detection, laser wavelength tuning for remote sensing, and so on.

4.4.1. Introduction

Multi-pass absorption cells consist of two identical spherical mirrors separated by nearly their radius of curvature. Laser beam is injected into the cell through a hole in one mirror, travels between the mirrors a certain number of times, and exits through a hole in the other mirror. The path length is changed by adjusting either the distance between the mirrors or the angle between the two axes of the mirrors. The beam spot pattern on the mirrors of the multi-pass absorption cell is changed by these factors as well. The beam spot pattern on the mirrors is a circular or elliptical shape in the case of spherical or parabolic mirrors. If we use astigmatic mirrors which are sometimes called 'toroidal mirrors' or 'asymmetric spherical mirrors', then the beam spot pattern on the mirrors is a Lissajous pattern. Astigmatic mirrors can make a longer path length than spherical or parabolic mirrors.[36]

The signal-to-noise ratio in laser spectroscopy or frequency modulation spectroscopy increases as the path length of laser beam does. However, the reflection losses of the mirrors and interference fringes limit the signal to noise ratio of detection. The interference fringes come from accidental etalons arising from the unwanted reflections between optical elements. This makes fringe patterns in the observed

signal and sometimes its width is the similar with the absorption signal. Therefore, it can be difficult to distinguish the absorption signal from the interference fringes. The interference fringe caused by a multi-pass absorption cell can be reduced effectively by various methods.[37]

4.4.2. Design

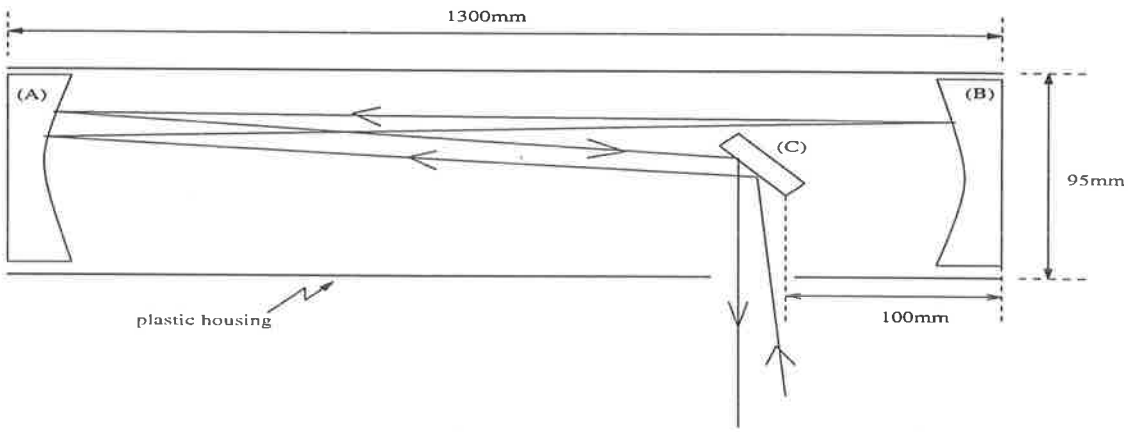

Figure 4.7 : Brief diagram of the multi-pass absorption cell. (A) and (B) are identical parabolic mirrors and (C) is a metal-coated flat mirror.

Our multi-pass absorption cell consists of two identical parabolic mirrors (diameter ≡ 95mm, radius of curvature ≅ 1.5m, metal coating), a metal-coated mirror (10mm×20mm×5mm), two mirror mounts, and plastic housing as shown in Figure 4.7. Our multi-pass absorption cell has no hole on the mirrors for the entrance and the exit of laser beam. Thus, the laser beam is injected into the cell through the entrance hole in the side of the plastic housing. The beam is reflected to one parabolic mirror by the flat mirror (C) and then, travels between the parabolic mirrors. Finally, the beam can exit the outside of the cell by means of the flat mirror (C).

Because there is a flat mirror between the parabolic mirrors, we do not need to make a hole on the parabolic mirrors and the number of spots on each mirror is different. The number of beam spots in mirror (A) of Figure 4.7 is one more than in mirror (B). The number of beam spots in mirror (A) was 9 and that of spots in mirror (B) was 8 in

our experiment. In addition, 24m of the optical path length was achieved by means of 1.3m of actual cell length.

The alignment of laser beam into the multi-pass absorption cell is usually not easy and a He-Ne laser can be helpful for this kind of alignment. The brief procedure for the alignment of the cell is, first, to make two parabolic mirrors approximately parallel to each other. Place the flat mirror (C) about 45 degrees to the co-axis of the parabolic mirrors. Second, using a He-Ne laser and the mirrors, i.e. M1, M2, and M3, align the beam into the cell as seen in Figure 4.8. We should see 9 spots in mirror (A) and 8 spots in mirror (B) to achieve 24m of the optical path length. The output beam must be reflected by M1 and should be observed after M1. Third, place two pinholes, PH1 and PH2, somewhere after and before M1. Lastly, using the master laser, another mirror M4, and beam splitter (BS), inject the beam through two pinholes. Of course, we can not move PH1, PH2, and M1 in order to maintain the path for the correct alignment but beam splitter (BS) can move horizontally and vertically. If it succeeds, then it means that the laser beam is almost properly aligned into the cell. Then, we adjust the mirrors a little to achieve the proper alignment.

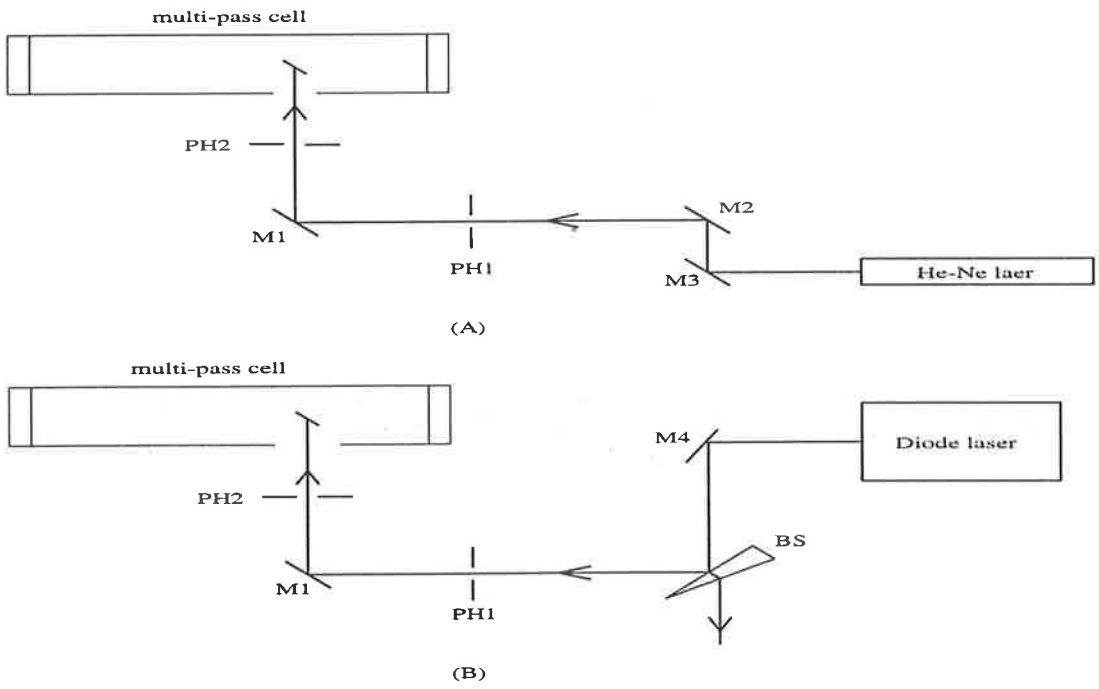

Figure 4.8 : Schematic for the alignment to the multi-pass absorption cell. M: mirror; PH: pinhole; BS : beam splitter

Chapter 5

Frequency modulation spectroscopy

There are two methods to observe water vapour absorption lines by means of lasers. First, we can observe water vapour absorption lines by 'direct measurement' with two photodiodes. Second, frequency modulation spectroscopy is another way to observe water vapour absorption lines.

In section 5.1, the brief schematics of direct measurement and frequency modulation spectroscopy are explained. In section 5.2, the absorption of laser power by water vapour is estimated in a certain condition. In section 5.3, the concept of frequency modulation spectroscopy including first and second harmonic detection is discussed.

5.1. Introduction

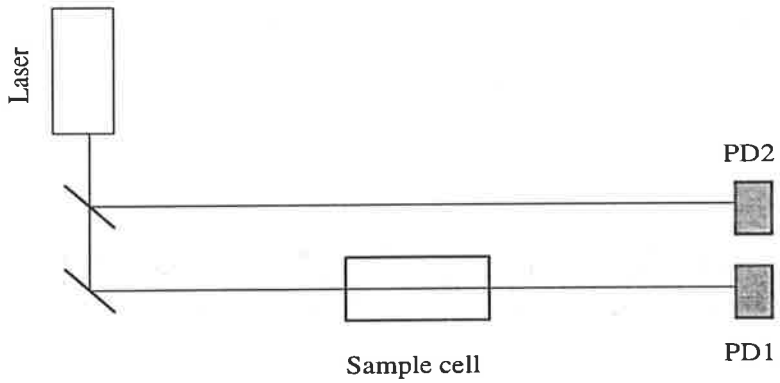

Figure 5.1: Schematic of direct measurement spectroscopy. Suppose that there is water vapour inside a sample cell.

We can directly detect the absorption of laser power by water vapour and schematic of direct measurement is shown in Figure 5.1. Let us call the laser beam passing through a sample cell 'signal beam' and the other beam 'reference beam' which does not travel through the cell. Suppose that the power of the two beams, i.e. the signal

and reference beams, are the same before the sample cell. The power of the signal beam after the sample cell will be smaller than that of the reference beam because some amount of the power of the signal beam was absorbed by water vapour. The laser beam can be chopped either mechanically or by an Acousto-Optic Modulator (AOM) and then, a lock-in amplifier or the other kind of phase-sensitive detector is used to detect the absorption of laser power by water vapour. The balance between the photodiodes is important to make the signal difference between the photodiodes zero, when there is no absorption by water vapour. It can be done either manually or using a balance circuit. When this balance procedure is performed, the wavelength of a laser must not be around water vapour absorption lines.

Interference fringe can be one of the major problems because it makes fringe patterns in the observed signal.[37,40] In addition, the width of the interference fringes is sometime similar as that of absorption lines so that it is difficult to distinguish the absorption lines from the interference fringes. In principle, it can be removed by means of a balance circuit, if the sources of the interference fringes are the same. However, the sources of the interference fringes for the signal beam and the reference beam are usually different and thus, it is very difficult to remove these interference fringes.

Frequency modulation spectroscopy can be a good alternative solution. First, frequency modulation spectroscopy uses only one detector. Therefore, we do not need to adjust the balance of the photodiodes either manually or automatically. In addition, frequency modulation spectroscopy has relatively a simple experimental setup and the wavelength locking of a laser to one of the absorption lines is easier using the error signal from a lock-in amplifier or a phase-sensitive detector.

In frequency modulation spectroscopy, the wavelength of a laser is modulated or scanned by two signals as shown in Figure 5.2. The frequency of one signal is much higher than the frequency of the other. The high and low frequency signals are called 'modulation signal' and 'scanning signal', respectively. In addition, the amplitude of the scanning signal is much higher than that of the modulation signal. If the modulated laser beam is scanned over absorption line, then the laser beam after the sample cell will undergo amplitude modulation caused by the absorption of water vapour. This amplitude modulation is in phase with the frequency of the modulation signal in the case of first harmonic detection, which will be discussed in section 5.3.

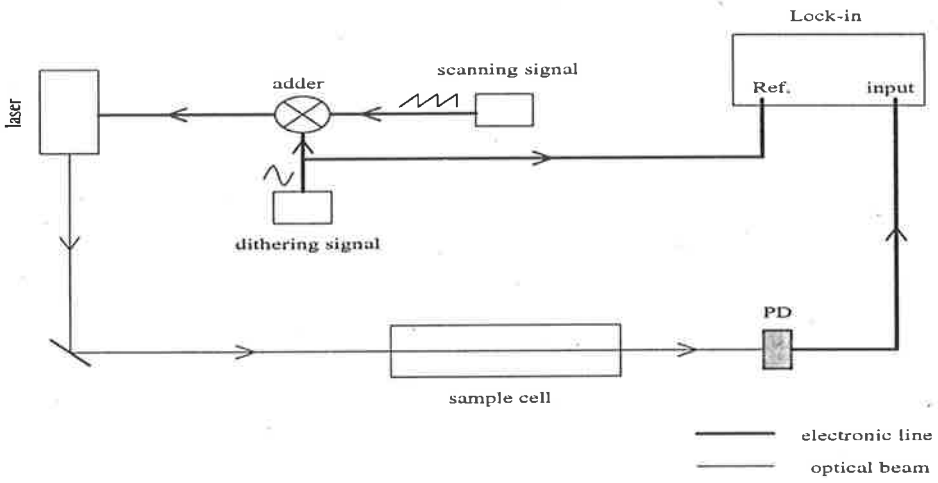

Figure 5.2: Schematic of frequency modulation spectroscopy. PD: photodiode, Ref.: reference input of a lock-in amplifier

5.2. Absorption of laser power by water vapour

The amount of laser power absorbed by water vapour, whose wavelength is around the centre of water vapour absorption line, is very small and depends on the wavelength of the laser. In this section, the amount of laser power absorbed by water vapour in a certain condition will be estimated using HITRAN database.

The wavelength of our laser is around 830nm. In this region, we do not need to worry about the absorption by nitrogen, oxygen, and the other gases that occupy more than 90% of air, because there is no absorption line by them around 830nm according to HITRAN database. Transmitted power ratio, T', can be defined as

$$T' = \frac{P_{out}}{P_{in}} = e^{-\rho L \sigma}, \qquad (5\text{-}1)$$

where ρ is the number density of water vapour, L is the path length of laser beam inside the sample cell, and σ is the absorption cross-section of water vapour. Sometimes $\rho L \sigma$ is called the optical depth of a molecule inside the cell.

If there is no water vapour, i.e. the number density of water vapour is zero, then P_{in} and P_{out} are the same. If water vapour is existing inside the sample cell and the

wavelength of laser is around the centre of water vapour absorption line, then P_{out} will be smaller than P_{in}. First, calculate the absorption cross-section of water vapour. The definition of cross-section, σ, is

$$\sigma = S \times f \tag{5-2}$$

where S is the line intensity of water vapour absorption line and f is the line shape function of water vapour.

The line shape function of the absorption line can be described by a Lorentzian when pressure or collisional broadening is dominant. The HWHM (Half Width at Half Maximum) of the line shape function in the lower atmosphere is about 0.1 cm^{-1} when pressure broadening is dominant.[12] In addition, when Doppler broadening is dominant, the line shape function is a Gaussian.[44] In the non-relativistic case, the Doppler shift, $\Delta\upsilon$, can be expressed as $\frac{u}{c} \cdot \upsilon_0$, where u is the velocity of molecules, c is the speed of light, and υ_0 is the centre wavenumber of absorption line. Suppose that the molecules are in thermodynamic equilibrium, then the statistics of the molecules can be described by Maxwell-Boltzmann distribution and the mean velocity of the molecules, $\bar{u}$, is given as $\sqrt{\frac{2kT}{m}}$, where k is Boltzmann constant, T is temperature, and m is mass of a molecule.[45] Using this mean velocity, the HWHM of the line shape function in the case of Doppler broadening is about 10^{-6} cm^{-1} in the lower atmosphere, which is much smaller than in the case of pressure broadening, 0.1 cm^{-1}. Therefore, in the lower atmosphere, the line shape function of water vapour absorption can be approximated with a Lorentzian as below,

$$f(\gamma, \upsilon) = \frac{1}{\pi} \frac{\gamma}{\gamma^2 + \upsilon^2}$$
$$\therefore f(\gamma = 0.1, \upsilon = 0) = 3.21 \tag{5-3}$$

where γ is the HWHM of line shape function and υ is deviation from the centre frequency of absorption line.[29,44]

Now, calculate the number density of water vapour using a hygrometer and pyschrometric chart. Suppose that dry-bulb temperature, T, is 20 °C and wet-bulb temperature is 13.5 °C. From these values and psychrometric chart, the partial pressure of water vapour, P, in the air can be obtained as about 1100 Pa. Absolute humidity, H_{abs}, can be calculated using ideal gas equation and its definition as below,

$$\begin{aligned} H_{abs} &= 2.2 \times \frac{P}{T} \\ &= 8.26 \ [\mathrm{g/m^3}]. \end{aligned} \tag{5-4}$$

Therefore, the number density of water vapour, ρ, is 2.76×10^{17} molecules/$\mathrm{cm^3}$ in this condition.

According to HITRAN database, one of the strongest water vapour absorption lines around 830nm is 1×10^{-23} cm/molecule so that let us use this line intensity to calculate the absorption cross-section of water vapour. If the path length of laser beam, L, is 24m, then the absorption cross-section of water vapour and the optical depth of water vapour, D, can be approximated as below,

$$\begin{aligned} &\sigma \cong S \times f(\gamma = 0.2, \upsilon = 0) = 1 \times 10^{-23} \times 3.21 = 3.21 \times 10^{-23} \ [\mathrm{cm^2/molecule}] \\ &\mathrm{D} = \rho \mathrm{L} \sigma = 2.76 \times 10^{17} \times 2.4 \times 10^{3} \times 3.21 \times 10^{-23} = 2.13 \times 10^{-2}. \end{aligned} \tag{5-5}$$

Therefore, the transmitted power ratio, T', is

$$\begin{aligned} T' &= \frac{P_{out}}{P_{in}} \\ &= e^{-2.13 \times 10^{-2}} \\ &= 0.978. \end{aligned} \tag{5-6}$$

That is to say, about 2% of the input power is absorbed by water vapour if the intensity of absorption line is 1×10^{-23} cm/molecule. According to HITRAN database,

the line intensities of most of the absorption lines around 800nm are less than 1×10^{-23} cm/molecule as shown in Figure 2.8.

5.3. Harmonic detection

As shown in Figure 5.2, the wavelength of a laser in frequency modulation spectroscopy is modulated (or dithered) and scanned at the same time. The transmitted signal after a sample cell can be detected by a phase-sensitive detector. If we apply the reference signal, which is the same frequency as that of modulation signal, to the phase-sensitive detector, then we can obtain the signal like the first derivative of the line-shape function of absorption line. If the frequency of the reference signal of the phase-sensitive detector is as twice as that of the modulation signal, then we can obtain the signal like the second derivative of the line-shape function of the absorption line. Therefore, frequency modulation spectroscopy is called sometimes either 'derivative detection' or 'harmonic detection'.

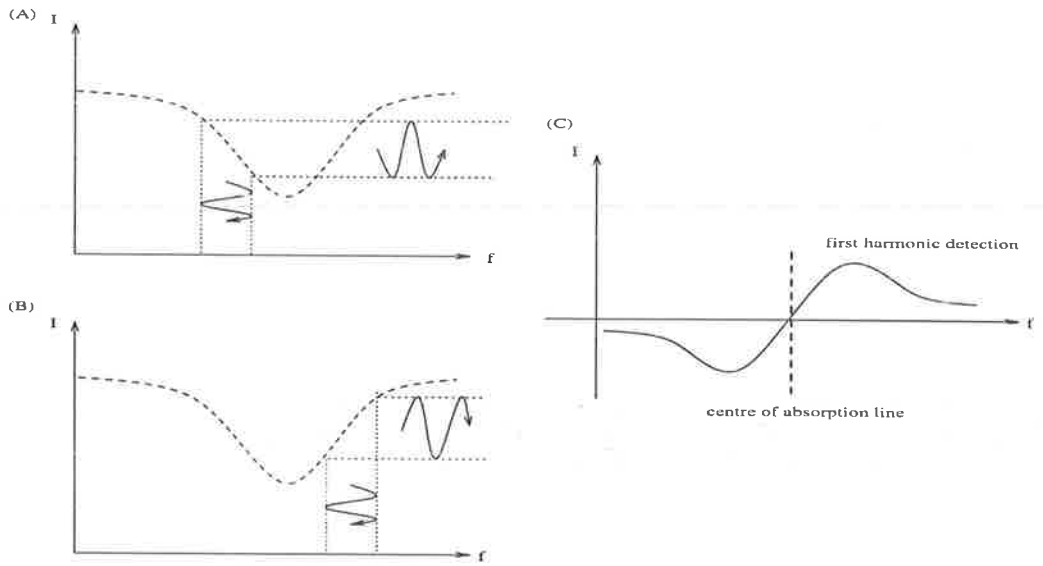

Figure 5.3 : Schematic diagram of frequency modulation spectroscopy. The intensity of laser is y-axis and the frequency of that is x-axis. Dashed line in (A) and (B) is the absorption line of a molecule and 'thick dashed line' in (C) represents the centre of absorption line.

There are two ways to explain how frequency modulation spectroscopy works. First way is that frequency modulation on a laser is converted into amplitude modulation after a sample cell. Figure 5.3 (A) and (B) represents the phase relation between the input laser's frequency modulation and the output beam's amplitude modulation. In Figure 5.3 (A), the laser is scanned from the left side of the absorption line, i.e. from smaller to larger frequency. In this case, the phase difference is 180 degrees. However, the phase difference is zero, when the right side of the absorption line is scanned as shown in Figure 5.4 (B).

Second, we can use an approximation to explain it. A more exact proof of this can be found in Ref. 32. Suppose that laser beam is transmitted through a sample cell. Obviously, the output intensity is a function of the frequency of a laser. Thus, the response function of molecules, $I_T(\upsilon)$, can be expressed as

$$I_T(\upsilon) = I_T(\upsilon + m\sin\Omega t) \tag{5-7}$$

where υ is the frequency of a laser, m is the amplitude of modulation signal, and Ω is the angular frequency of modualtion signal.

If m and Ω are smaller than the linewidth of the absorption line, the response function of molecules, $I_T(\upsilon)$, can be written approximately,

$$I_T(\upsilon + m\sin\Omega t) = I_T(\upsilon) + (m\sin\Omega t)\frac{dI_T}{d\upsilon} + \left(\frac{m^2\sin^2\Omega t}{2!}\right)\frac{d^2I_T}{d\upsilon^2}\cdots \tag{5-8}$$

and after combining terms,

$$\begin{aligned} I_T(\upsilon + m\sin\Omega t) = &\left[I_T(\upsilon) + \frac{m^2}{4}\frac{d^2I_T}{d\upsilon^2}\cdots \right] \\ &+ \sin\Omega t\left[m\frac{dI_T}{d\upsilon} + \frac{m^3}{8}\frac{dI_T{}^3}{d\upsilon^3}\cdots \right] \\ &+ \cos 2\Omega t\left[-\frac{m^2}{4}\frac{d^2I_T}{d\upsilon^2}\cdots \right] + \cdots . \end{aligned} \tag{5-9}$$

The transmitted intensity has 'dc term' and 'oscillating terms' whose frequencies are $\Omega, 2\Omega, 3\Omega \cdots$. If we use a phase-sensitive detector, then the coefficient of the oscillating term at a certain frequency – the frequency of the reference signal of the phase-sensitive detector – can be detected. For example, if the frequency of the reference signal of the phase-sensitive detector is the same as that of modulation signal, i.e. Ω, then we can obtain the coefficient of $\sin \Omega t$. In addition, if m is small enough to ignore the higher order derivative of $I_T(\upsilon)$, the coefficient of $\sin \Omega t$ is approximately the same as the first derivative of the line-shape function of absorption line. This is called 'first harmonic detection'. Similarly, if phase-sensitive detector's reference frequency is 2Ω, then the coefficient of $\cos 2\Omega t$ can be obtained and this method is called 'second harmonic detection'.

Figure 5.4 (A) and (B) are schematic diagrams to show the cases of first and second harmonic detection. In the case of first harmonic detection, the zero crossing point of the signal is the centre of the absorption line. The middle peak of the signal is the centre of the absorption line in the case of second harmonic detection as shown in Figure 5.4 (B).

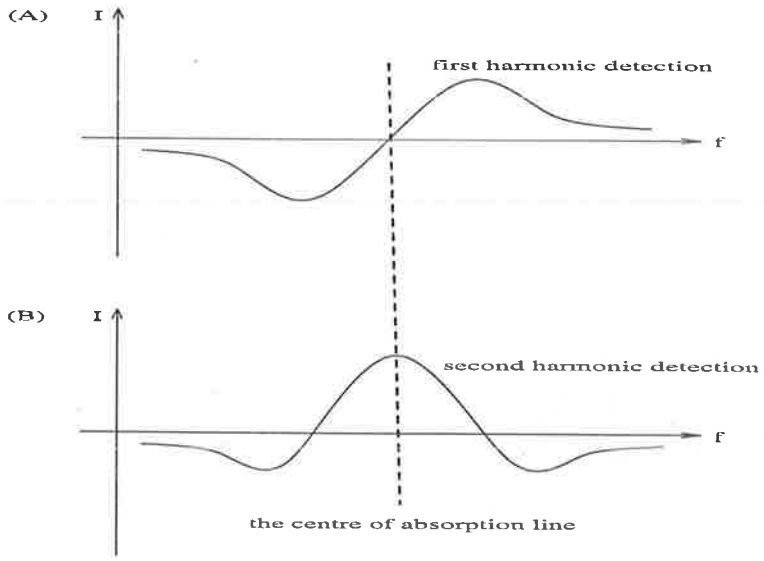

Figure 5.4 : Schematic diagram to explain first and second harmonic detection.

Chapter 6

Experiment ||
Water vapour detection

This chapter is about water vapour detection experiments by frequency modulation spectroscopy and the wavelength locking of the master laser of our DIAL system to the centre of water vapour absorption line. In section 6.1, intensity modulation method is discussed briefly. In section 6.2, first harmonic detection for investigating water vapour absorption lines is discussed. In section 6.3, absolute humidity is measured using the results of first harmonic detection. In section 6.4, second and first harmonic detection in the cases of various modulation signals is discussed. In section 6.5, the master laser's wavelength locking to the centre of water vapour absorption line and frequency stability of the wavelength of the master laser are discussed.

6.1. Intensity modulation method

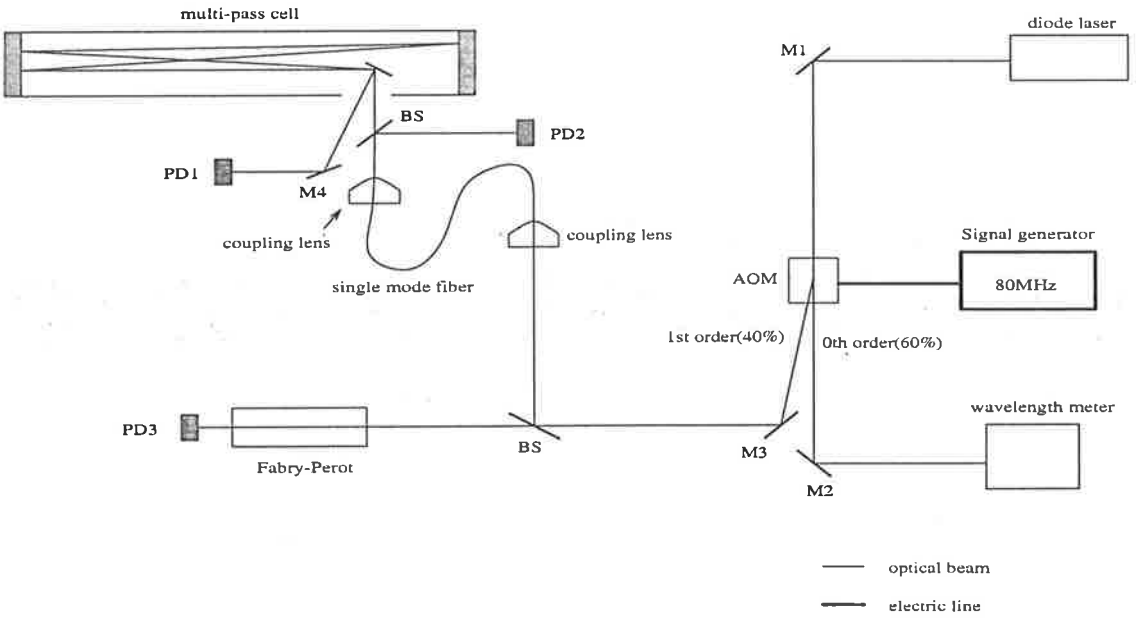

Figure 6.1 : Experimental setup for intensity modulation method. PD : photodiode; M : mirror; BS : beam splitter; AOM : Acousto-Optic Modulator

Figure 6.1 is the experimental setup for intensity modulation method to detect water vapour absorption lines. First, laser beam is transmitted into an Acousto-Optic Modulator (AOM, Isomet MOD 1205-630F). The power of the first order of the AOM is about 40 % of the input power. There are two roles for the AOM. One is to chop the laser beam when we use intensity modulation method. The other role is that the AOM can isolate the diode laser from feedback which comes from Fabry-Perot or a fibre coupling lens. The zeroth order of the AOM is going to a wavelength meter (ILX Lightwave LWM-6500B). Because the feedback from this wavelength meter is not strong, we can use the zeroth order of the AOM for that. The first order of the AOM is going to both a confocal scanning Fabry-Perot and a fibre coupling lens. After the coupling lens, the laser beam is aligned into the multi-pass absorption cell and some portion of the laser beam is going to PD2 (UDT PIN-6DI) before the absorption cell. The output of PD2 can be used as the reference signal in order to remove interference fringes. In addition, the output beam of the cell is going to PD1 (UDT PIN-6DI). The current of the diode laser is fixed and conversely, the temperature of the diode laser is scanned by the external port of the temperature controller. A function generator (Wavetek model 164) supplies triangle signal to the external port of the temperature controller and the frequency of that is 0.002Hz.

80MHz sinusoidal wave from a signal generator (Rohde & Schwarz, SMX) is supplied to the AOM. In addition, square wave from the other function generator (HAMEG 8030) is supplied to the external port of the signal generator (Rohde & Schwarz, SMX). The frequency of this square wave, i.e. the frequency of the chopping signal, is about 100Hz. In other word, the amplitude of 80MHz sinusoidal wave from the signal generator is modulated at the rate of about 100Hz by means of this square wave. The signal from either PD1 or the photodiodes is going to the input of a lock-in amplifier (Stanford Research System, SR510) and the trigger output (TTL) of the function generator, which produces the square wave for chopping, is used as the reference signal of this lock-in amplifier.

'Unbalanced signal (PD1)', which is the output of the lock-in amplifier, is shown in Figure 6.2. A peak around 30s may be interpreted as one of water vapour absorption lines. However, it is not clear and the baseline of this signal changes very much compared with the amplitude of the absorption signal. In addition, we can see many fringe patterns in Figure 6.2. Some patterns may not be the interference fringes but be

water vapour absorption lines. To remove this interference fringes, we used the signal from PD2 as the reference signal. In other word, 'balanced signal (PD2-PD1)' was used as the input of the lock-in amplifier. However, the amplitude of the interference fringes was increased. That might be because the sources of the interference fringes were different in the cases of PD1 and PD2.

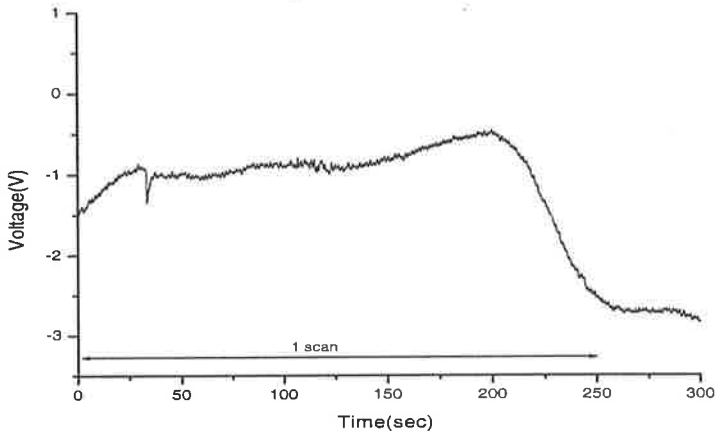

Figure 6.2 : The output of the lock-in amplifier (PD1) in the case of intensity modulation. Period of scanning : 250 (s); wavelength : 834.5 – 833.6 (nm); sensitivity of lock-in : 2 (mV); time constant of lock-in : 100 (ms).

6.2. First harmonic detection

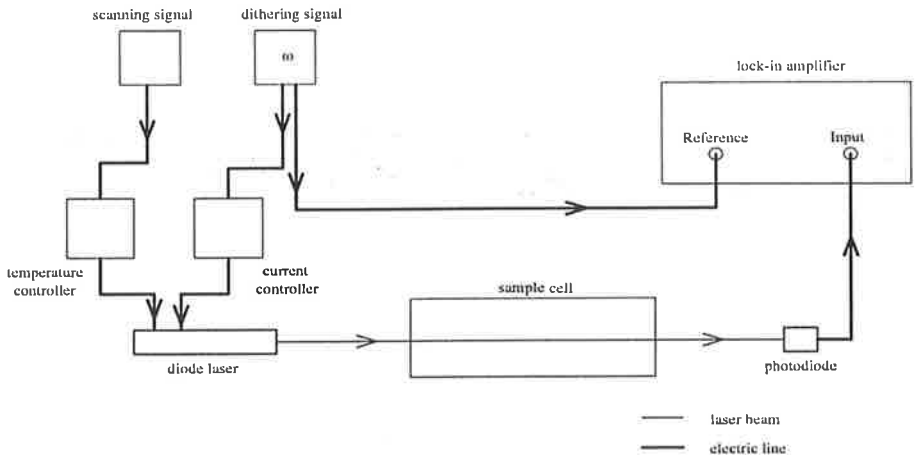

Figure 6.3 : Basic schematic of frequency modulation spectroscopy. The scanning and dithering signals can be summed and delivered to the current controller alone.

In the previous section, we did not obtain good water vapour absorption signals using intensity modulation method and a main problem came from the interference fringes. In this section, we will use frequency modulation method to detect water vapour absorption lines. Frequency modulation spectroscopy makes it possible to detect a small amount of molecules as discussed in Chapter 5.[41] In frequency modulation spectroscopy, the wavelength of a laser is scanned - the order of hundreds of GHz - and dithered - the order of hundreds of MHz - at the same time by the external modulation port of temperature or current controller as shown in Figure 6.3. Mode-hop can be a serious problem in frequency modulation spectroscopy because the continuous wavelength scanning is difficult. However, it is possible to avoid the mode-hops by choosing a suitable diode laser and finding suitable temperature and current of the diode laser.

To reduce these interference fringes, we designed a new experimental setup as shown in Figure 6.4. This new setup is basically the same as the previous one, Figure 6.1, but there are two major differences. First, the number of optics between the diode laser and the multi-pass absorption cell is reduced. Second, a single mode optical fibre is not used to deliver laser beam into the multi-pass absorption cell in order to avoid the interference fringe from it. In this experimental setup, laser beam travels to a wedge and some of the laser beam is delivered to the multi-pass absorption cell. A Faraday isolator (New Focus, #5567) is used because it can prevent the optical feedback that is caused by Fabry-Perot.

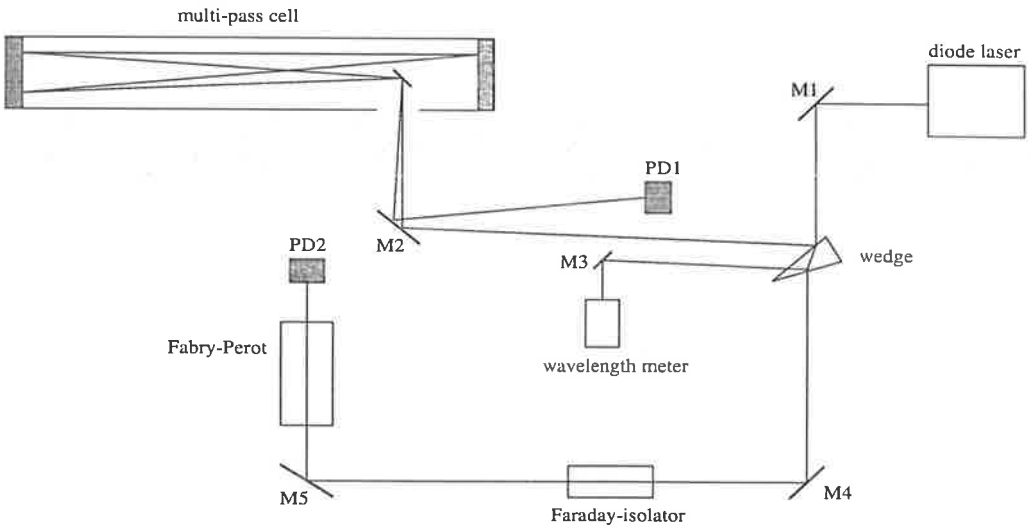

Figure 6.4 : An experimental setup for first harmonic detection

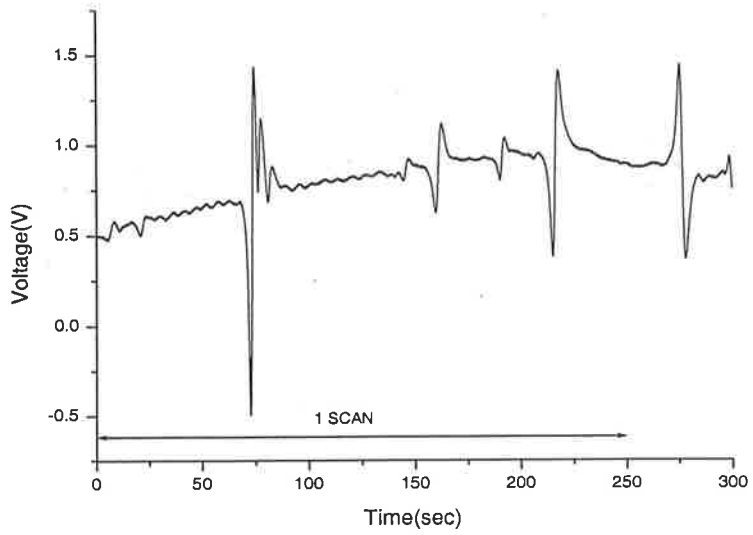

Figure 6.5 : Water vapour absorption lines. Period of scanning: 250 (s); frequency of dithering: 440 (Hz); temperature: 290.4–304.1 (K); wavelength: 832.6–833.7 (nm); sensitivity of lock-in : 200 (μV); time constant : 100 (ms)

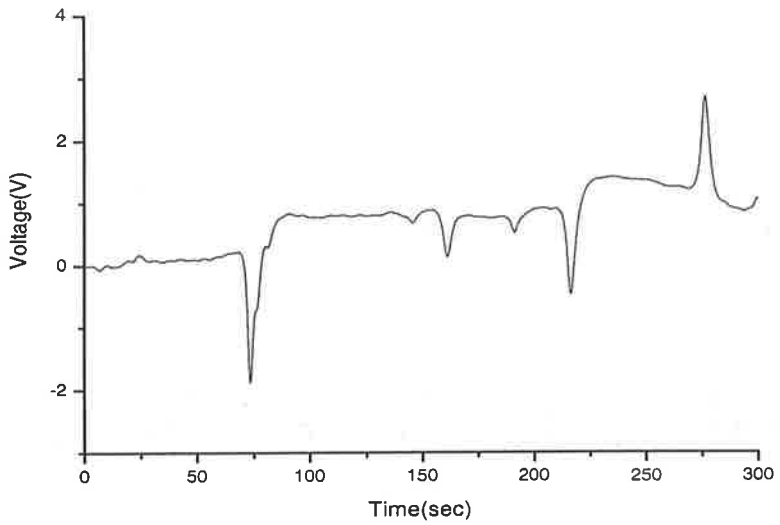

Figure 6.6 : Integrated data of Figure 6.5.

In Figure 6.5, the frequency of the diode laser is scanned several tens of GHz and dithered about hundred MHz. Four peaks can be resolved in Figure 6.5 and those peaks are the first derivatives of the water vapour absorption lines. The first

absorption line looks like the superposition of two or three absorption lines and small interference fringes can be seen. The wavelength of the diode laser is scanned by the external port of the temperature controller and the period of the scanning is 500s. The last two resonances are the same water vapour absorption lines and thus, the shape of these lines are opposite each other. For the same reason, the integrated signals of these signals shown in Figure 6.6 are opposite as well.

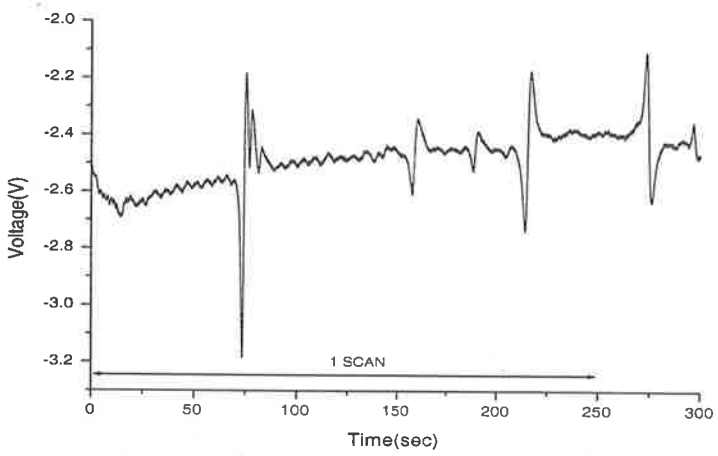

Figure 6.7 : Water vapour absorption lines in the case of ambient air. Every condition is the same as Figure 6.8.

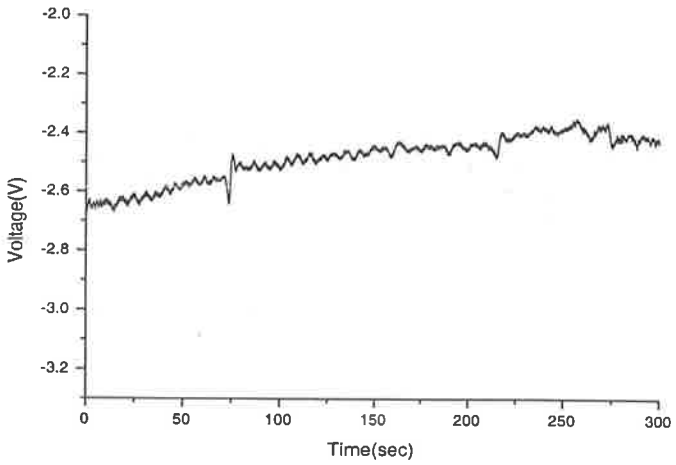

Figure 6.8 : Water vapour absorption lines when the multi-pass cell is full of dry nitrogen gas. Every condition is the same as Figure 6.7.

If we can control the amount of water vapour inside the absorption cell, then it is much clearer whether the peaks in Figure 6.5 are water vapour absorption lines or not. To do this, we supply dry nitrogen gas to the multi-pass absorption cell. According to the manufacturer, this nitrogen gas (BOC, high purity nitrogen) has less than 100 ppm of water vapour. Figure 6.7 and Figure 6.8 are the water vapour absorption lines when the cell is opened to air and when it is full of dry nitrogen gas, respectively. From Figure 6.7 and 6.8, we can know the amplitude of water vapour absorption lines in the case of dry nitrogen gas is much smaller than in the case of ambient air. Therefore, we can say that these peaks are definitely the water vapour absorption lines around 830nm.

Before we scan the wavelength of the laser over a single water vapour absorption line only with the external modulation port of the current controller, we can find the centre wavelength of the observed water vapour absorption lines. The measurement error of the wavelength meter (ILX Lightwave LWM-6500B) is about 0.5nm according to the manufacturer so that we can not measure the centre wavelength of the observed absorption lines with this wavelength meter as precise as we want.[42] However, if we compare the frequency difference between the observed absorption lines with HITRAN database, then we can find the centre wavelength of each water vapour absorption line. In the second experiment of this section, every condition is the same as the first experiment, except that no ramp signal is supplied to the Piezo of Fabry-Perot to find the frequency difference between the centres of the observed water vapour lines using Free Spectral Range (FSR) of Fabry-Perot.

Two water vapour absorption lines can be observed in Figure 6.9 and the frequency difference between the centres of the absorption lines is about 67.5 GHz. To find the centre wavelength of each absorption line, we should compare the data with HITRAN database. Therefore, we need at least three water vapour absorption lines at one data set. About ten water vapour absorption lines were observed from our experiments and we could find the wavelengths of seven water vapour lines as shown in Figure 6.12 and 6.14.

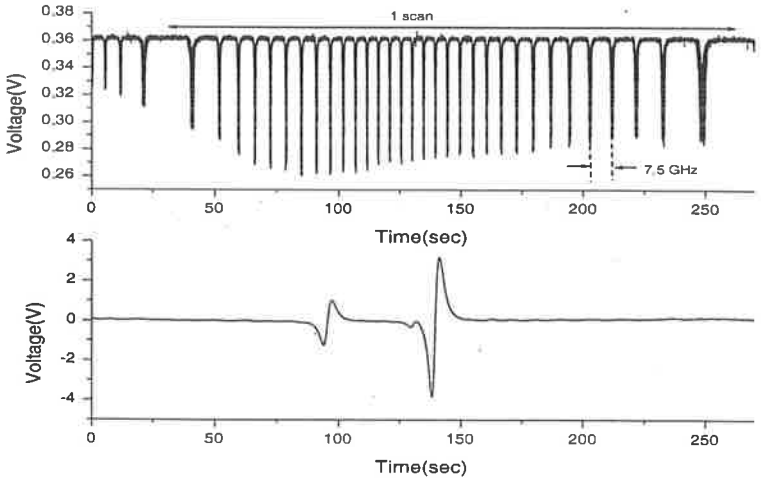

Figure 6.9 : Water vapour absorption lines. The upper data are from Fabry-Perot and the lowers are the output of the lock-in amplifier. Period of scanning: 250 (s); wavelength: 830.1-828.2 (nm); temperature: 289.2-280.6 (K); power of diode laser: 12.1-12.5 (mW); sensitivity of lock-in: 200 (μV); time constant of lock-in: 100 (ms)

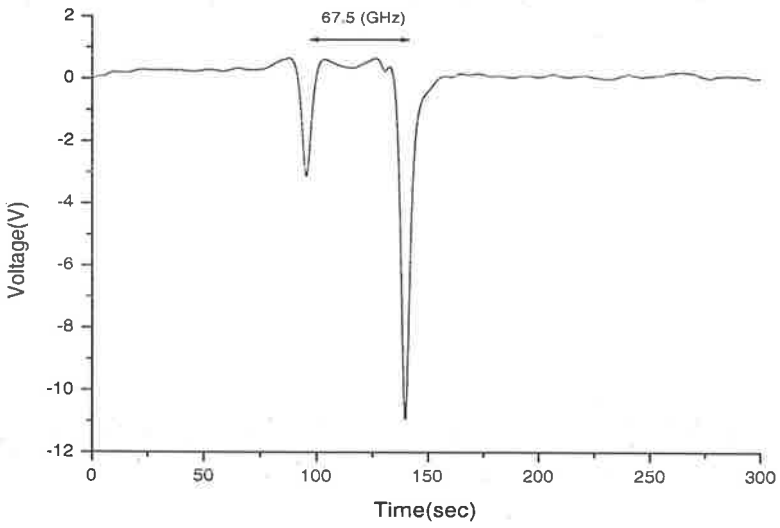

Figure 6.10 : Integrated data of Figure 6.9

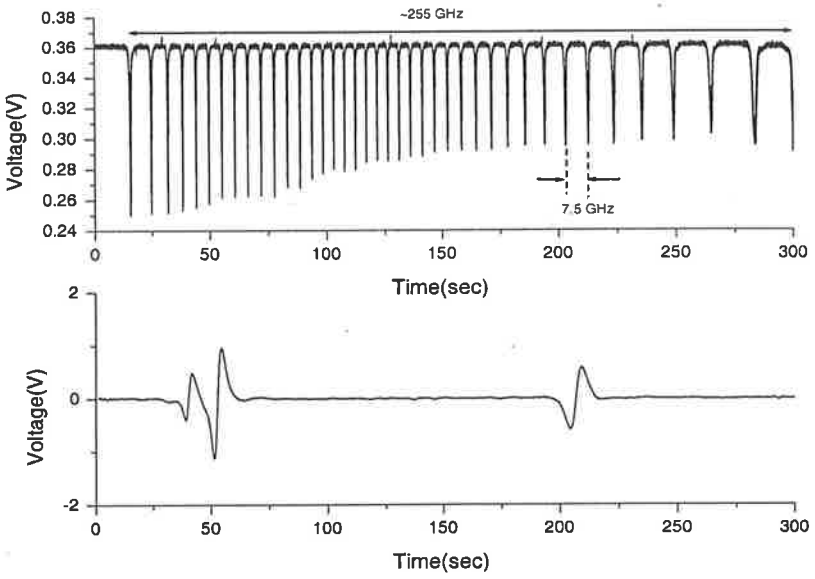

Figure 6.11 : Water vapour absorption lines. Period of scanning: 250 (s); wavelength: 829.3-828.4 (nm); temperature: 288.9-279.8 (K); power of diode laser: 12.1-12.6 (mW); sensitivity of lock-in: 100 (μV); time constant of lock-in: 100 (ms)

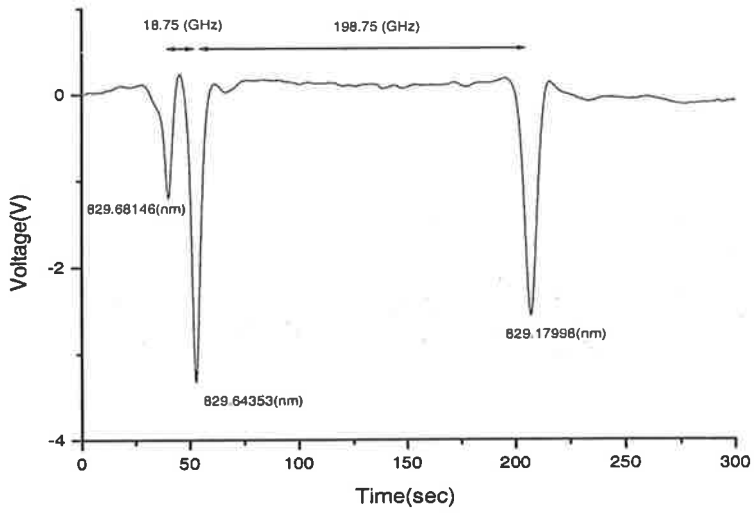

Figure 6.12 : Integrated data of Figure 6.11

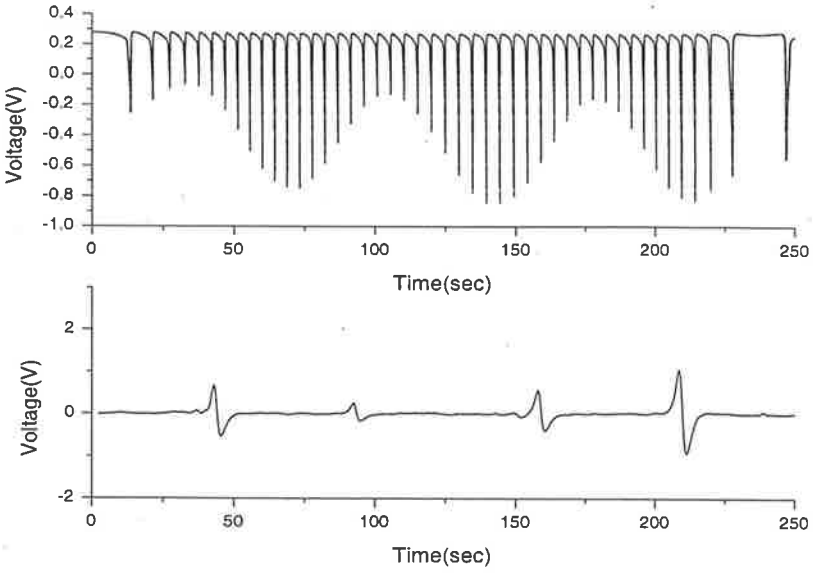

Figure 6.13 : Water vapour absorption lines. Period of scanning: 250 (s); wavelength: 831.0-831.9 (nm); temperature: 283.7-295.8 (K); power of diode laser: 20.7-20.1 (mW); sensitivity of lock-in: 100 (μV); time constant of lock-in: 100 (ms)

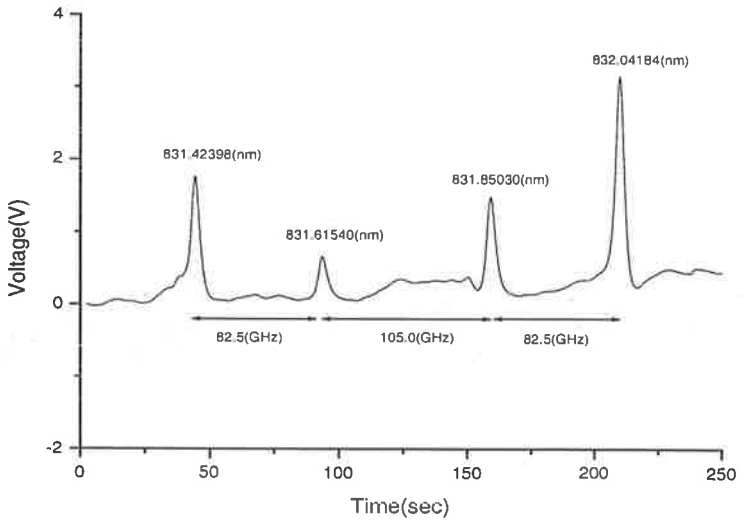

Figure 6.14 : Integrated data of Figure 6.13

Wavelength [nm]	Intensity [$cm^{-1}/molecule \cdot cm^{-2}$]
829.68146	6.03×10^{-24}
829.64353	1.67×10^{-23}
829.17998	9.57×10^{-24}
831.42398	6.20×10^{-24}
831.61540	2.11×10^{-24}
831.85030	6.33×10^{-24}
832.04184	1.45×10^{-23}

Table 6.1: Wavelength and intensity of the observed water vapour absorption lines.

Wavelength [nm]	Relative intensity (Experiment)	Relative intensity (Theory)
829.68146	0.40	0.36
829.64353	1	1
829.17998	0.78	0.57

Wavelength [nm]	Relative intensity (Experiment)	Relative intensity (Theory)
831.42398	0.57	0.43
831.61540	0.21	0.15
831.85030	0.43	0.44
832.04184	1	1

Table 6.2: Relative intensities in the cases of experimental measurements and theoretical calculations from HITRAN database.

According to the HITRAN database, the intensity of the first absorption line in Figure 6.13 is a little smaller than that of the third absorption line. However, in our measurement, the intensity of the first peak is bigger than that of the third peak. It may be caused by the variation of the baseline or the other water vapour absorption lines that are close to 831.42398nm.

The next step is to find a single water vapour absorption line to lock the wavelength of the laser to the centre of that. The deviation of the wavelength of the laser from the centre of water vapour absorption line should be smaller than 200MHz as shown in Table 2.1. We use the output of a lock-in amplifier to lock the wavelength of the master laser. First, we should be able to scan the wavelength of the laser over a single water vapour absorption line. In addition, we had better scan and modulate the wavelength of the laser by means of only one method, i.e. either current or temperature. However, we can not modulate the wavelength of the laser with a temperature controller in the speed of about 100Hz. Therefore, temperature is fixed and the wavelength of the laser is scanned and modulated by means of the external port of the current controller. A summing circuit in Figure 6.15 is constructed with operational amplifiers (OP-27). Two signals, i.e. sinusoidal and triangle, are added after this circuit.

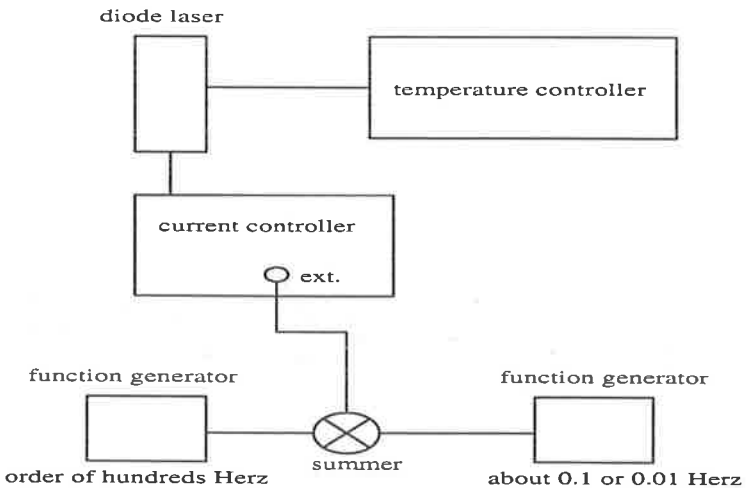

Figure 6.15 : Schematic for scanning and modulating the wavelength of the diode laser only with the external port of the current controller.

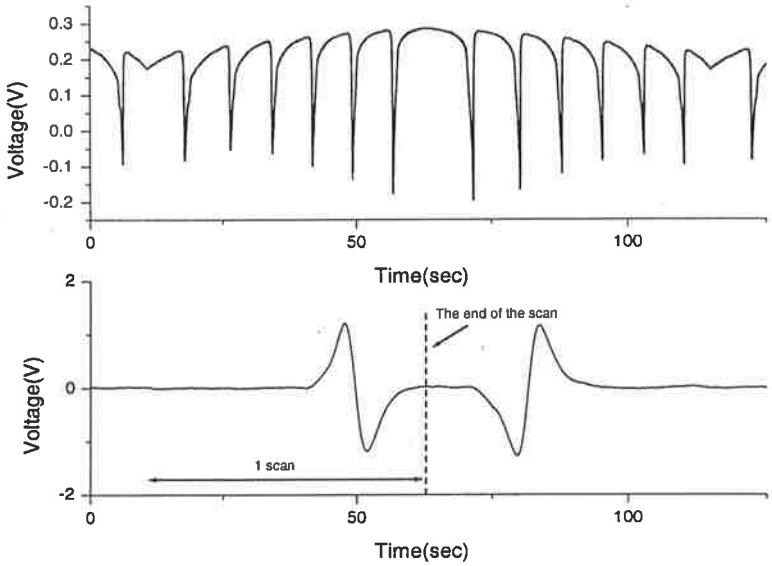

Figure 6.16 : Single water vapour absorption line. Period of scanning: 50 (s); wavelength: 832.1-831.5 (nm); temperature: 295.2 (K); power of laser: 24.3-15.6 (mW); current : 90.9-67.2 (mA); sensitivity of lock-in: 100 (μV); time constant of lock-in: 100 (ms)

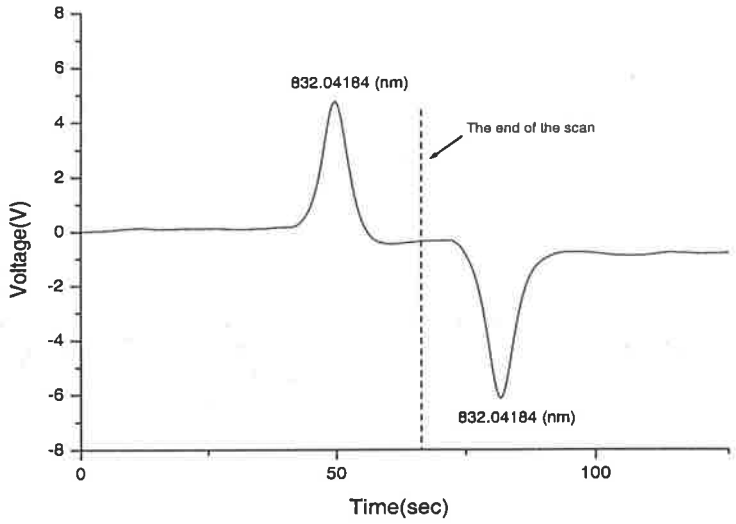

Figure 6.17 : Integrated data of Figure 6.16

A single water vapour line is shown in Figure 6.16 and Figure 6.17. The centre wavelength of this water vapour absorption line is 832.04184 nm. This wavelength is found using information from Figure 6.14 and Table 6.1. In other word, we first set the temperature and current of the diode laser to 295 K and 20 mW, respectively, according to information obtained from the previous experiments. Then, scan the wavelength of the laser using the current controller and adjust the range of scanning until the water vapour absorption lines is observed. To make sure that the wavelengths of this absorption line is 832.04184 nm, if the temperature of the diode laser is turned down, then the other water vapour absorption lines as shown in Figure 6.14 should be observed. During the scanning of the laser by the current controller, the current and power of the diode laser are changed about 23mA and 9mW, respectively.

6.3. Absolute humidity

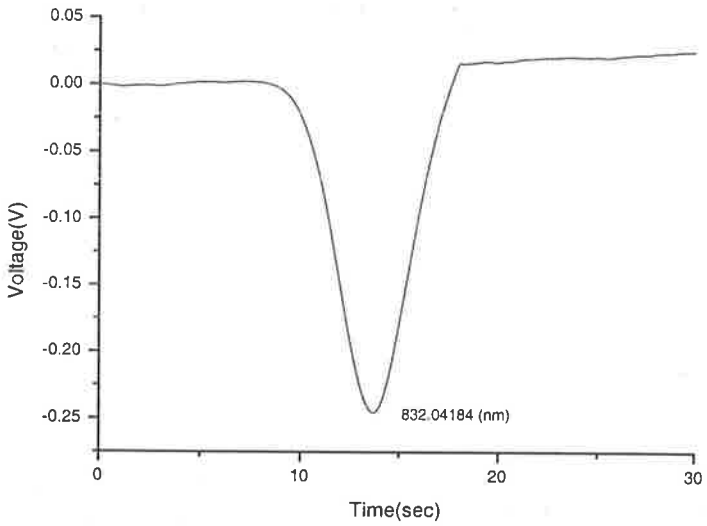

Figure 6.18 : Integrated data of the signal of first harmonic detection. The centre wavelength of the absorption line is 832.04184 nm

The water vapour absorption line in 832.04184nm was measured by frequency modulation method as shown in Figure 6.18. We can calculate absolute humidity from this and compare it with the value measured by a hygrometer. The amplitude of this

observed absorption line depends on both 'modulation index' and the gain of a lock-in amplifier. Modulation index, m, can be defined and measured as below,

$$m = \frac{\Delta\gamma'}{\Delta\gamma} = \frac{250\,\text{MHz}}{3\,\text{GHz}} \cong 0.08 \tag{6-1}$$

where $\Delta\gamma$ is HWHM (Half Width at Half Maximum) of absorption line shape function and $\Delta\gamma'$ is the amplitude of modulation. The gain of the lock-in amplifier (Stanford Research System, SR510) can be measured by applying a test signal to the input of the lock-in amplifier. The amplitude of the output of the lock-in amplifier is 10V when that of the input is 16 mV and the sensitivity of the lock-in amplifier is 1mV. Therefore, the gain of lock-in amplifier is $\frac{10000}{16} = 625$.

The amplitude of the absorption line is measured as 0.25 V and the real amplitude of this absorption line can be measured using modulation index and the gain of the lock-in amplifier. The real amplitude of this absorption line is obtained as 5 mV and the dc level of the output of the photodiode is 268 mV. Using the two values, we can obtain transmitted power ratio, T',

$$T' = \frac{P_{out}}{P_{in}} = 0.981 \tag{6-2}$$

Now we can obtain the number density of water vapour, ρ, and absolute humidity, H_{ab}, by Eq. (5-1),

$$\rho = -\frac{\ln(T')}{\sigma \cdot L} = 1.8\times10^{17}\ [\text{molecules/cm}^3] \tag{6-3}$$

$$\therefore H_{ab} = 5.11\ [\text{g/m}^3]$$

where L $(=2400\,cm)$ is the path length of our multi-pass absorption cell and σ is the absorption cross section of water vapour. The uncertainty of this measurement, $\left|\frac{\Delta\rho}{\rho}\right|$, can be estimated in the case of $\Delta T' = 0.001, \Delta L = 10$ and $\Delta m = 0.007$,

$$\begin{aligned}\left|\frac{\Delta\rho}{\rho}\right| &= \frac{1}{\ln(T')}\frac{\Delta T'}{T'} + \frac{\Delta L}{L} + \frac{1}{\ln(T')}\frac{1}{T'}\frac{0.001}{m^2}\Delta m \\ &= 0.054 + 0.004 + 0.059 \\ &= 0.117\end{aligned} \tag{6-4}$$

and then, the relative uncertainty of this measurement is 11.7 % and absolute humidity can be measured

$$\therefore H_{ab} = 5.11 \pm 0.60 \ [\mathrm{g/m^3}]. \tag{6-5}$$

The next step is to measure absolute humidity using a hygrometer. Absolute humidity measured by a hygrometer, H_{ab}', can be defined in terms of partial pressure of water vapour, P, and dry temperature, T,

$$H_{abs}' = 2.2 \times \frac{P}{T} \tag{6-6}$$

We measured dry and wet temperature ten times and from these data we could also obtain the uncertainty of this measurement. Thus, absolute humidity measured by a hygrometer, H_{ab}', is

$$H_{abs}' = 7.82 \pm 0.47 \ [\mathrm{g/m^3}]. \tag{6.7}$$

There is difference between two measurements, H_{ab} and H_{ab}'. There may be three sources of errors. First, we use the absorption line strength from HITRAN database to calculate the absorption cross-section of water vapour, σ, and this value may not be

correct. Second, the measurement of the modulation index in the frequency modulation spectroscopy can be incorrect. Third, there are random errors when we measure dry and wet bulb temperature or partial pressure of water vapour from psychrometric chart.

6.4. Second harmonic detection

Second harmonic detection gives us flatter baseline and bigger amplitude of signal and thus, this method is useful in some applications, for example gas detection.[32] The difference between first and second harmonic detection is whether the frequency of the reference signal of a phase-sensitive detector is the same or twice as that of the modulation signal. In the case of second harmonic detection, the frequency of the reference signal is doubled by the phase-sensitive detector. Figure 6.19 and Figure 6.20 are the outputs of the lock-in amplifier in the cases of first and second harmonic detection, respectively. Every condition is the same, except of the amplitude of modulation, because bigger amplitude of the modulation signal is needed in the case of second harmonic detection.[32] As we expect, the output of the lock-in amplifier in the case of second harmonic detection is like the second derivative of absorption line. In the case of first harmonic detection, the zero crossing point is the centre of absorption line. In the case of second harmonic detection, the centre peak of signal is the centre of absorption line. In Figure 6.19, the two peaks represent the same water vapour absorption line and the shape of the two signal is opposite because the direction of scanning is opposite. Therefore, two peaks in Figure 6.20 should be opposite as the case of first harmonic detection. However, in our measurement, these two peaks in Figure 6.20 and Figure 6.21 are not opposite each other.

According to the numerical calculation of harmonic detection in cases of various modulation waveforms, the best signal is obtained by the use of triangle waveform.[40] We tried three kinds of waveforms – sinusoidal, triangle and square. In our experiment, the amplitude of signal in the use of triangle waveform was smaller than in the case of sinusoidal waveform as shown in Figure 6.21. In the case of square waveform, the signal was distorted and it was not possible to observe absorption lines. Hovde et al reported the same kind of problem in Ref. 41. There are two main reasons

for this. First, the finite bandwidth of a current supplier or a summing amplifier circuit can distort the modulation waveform. In other word, although we give triangle waveform as the modulation signal to the current controller of the diode laser, the actual waveform to the diode laser, i.e. the output of the current controller, can be distorted. Second, the variation of the current makes the temperature of the diode laser vary, especially around the junction of the diode laser, and this temperature variation can make the change of the frequency of the laser. More investigation of this problem needs other experiments, in which different amplitudes, kinds and frequencies of modulation waveforms should be supplied to the laser.

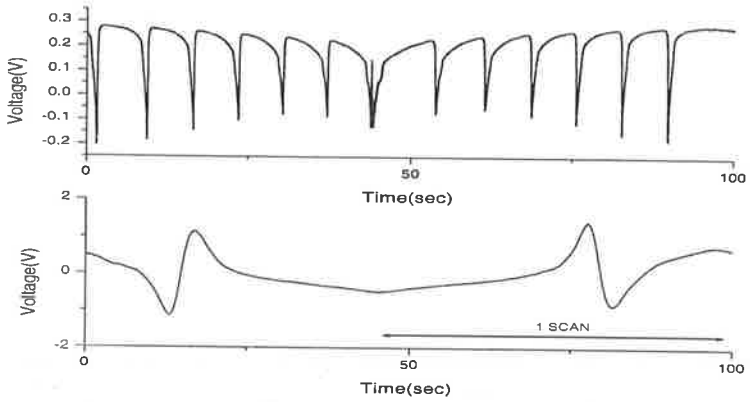

Figure 6.19 : First harmonic detection of water vapour absorption line. Period of scanning: 50 (s); wavelength: 831.5-832.0 (nm); temperature: 294.9 (K); power of laser: 14.9-24.5 (mW); current of laser: 65.5-91.0 (mA); sensitivity of lock-in: 20 (μV); time constant of lock-in: 300 (ms)

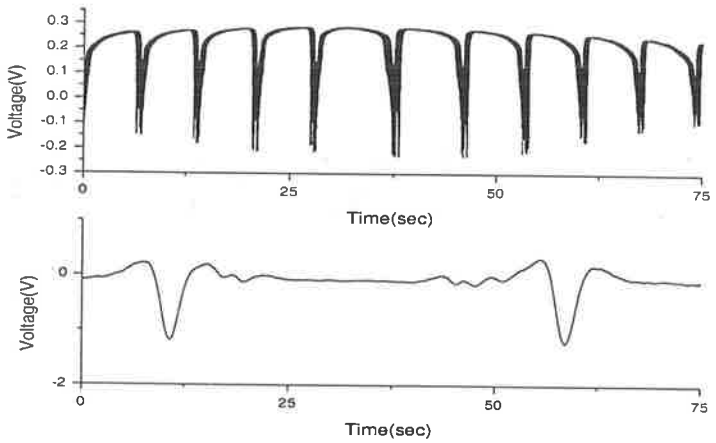

Figure 6.20 : Second harmonic detection of water vapour absorption line. Every condition is the same as Figure 6.19 except the amplitude of dithering is bigger.

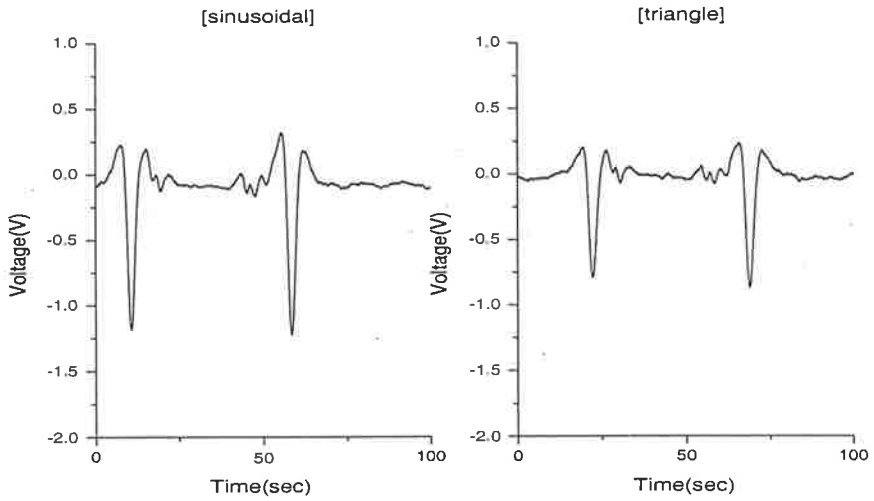

Figure 6.21 : Second harmonic detection in the cases of sinusoidal and triangle modulation waveform

6.5. Laser wavelength locking to water vapour absorption line

Several water vapour lines were observed by means of first and second harmonic detection. Additionally, the wavelengths and line intensities of seven absorption lines were found by comparing experimental data with theoretical calculations, i.e. HITRAN database.

Schematic of wavelength locking is to use the output of a phase-sensitive detector as the feedback signal to the current controller of the diode laser. In other word, we use the fact that the zero-crossing of the first derivative of water vapour absorption line represents the centre of absorption line. For example, if the wavelength of the laser is exactly on the centre of the absorption line, then the output of the phase-sensitive detector is zero. Otherwise, the output of the phase-sensitive detector is positive or negative as shown in Figure 6.22. This error signal from the phase-sensitive detector is integrated inversely and it leads the current of the laser toward that of the centre wavelength of the water vapour absorption line. For example, if the set-point of the external port of the current controller is bigger than that of the centre of the absorption line, then the error signal from the phase-sensitive detector is positive and thus, the inversely integrated signal of this error signal is negative as shown in Figure 6.22.

Therefore, the current to the laser decreases in order to reach the current for the centre of the absorption line.

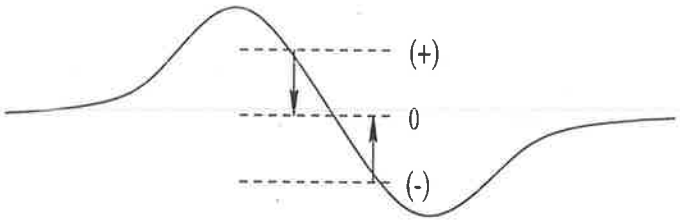

Figure 6.22 : Schematic of wavelength locking

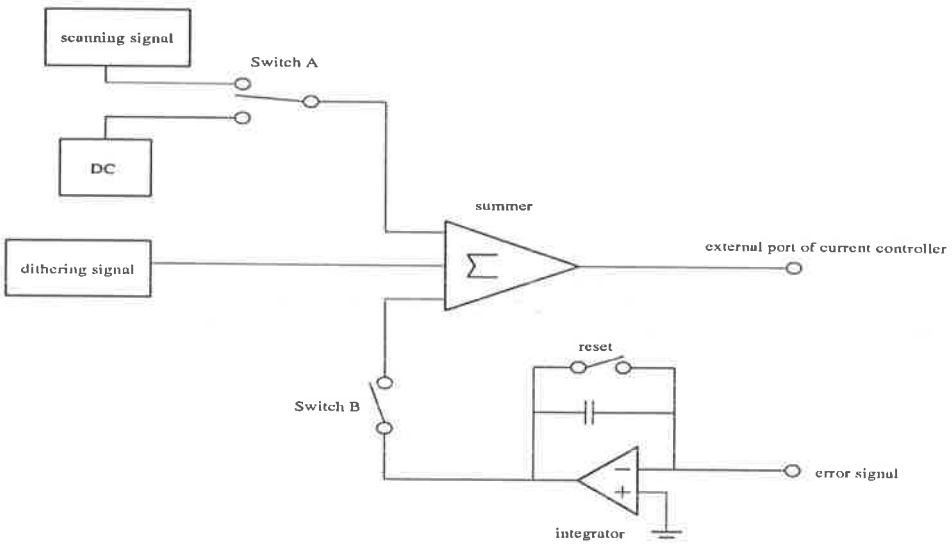

Figure 6.23. Simple diagram of the wavelength locking circuit

The simple diagram of the current locking circuit is in Figure 6.23 and the circuit diagram of this wavelength locking circuit can be found in Appendix A. There are four signals, which are scanning, dithering, dc, and integrated error signals. The signals are added by a summing amplifier and delivered to the external port of the current controller. A switch in the integrating part is to make the output of the integrating amplifier zero at the start of integration. The procedure for wavelength locking is first using the scanning and dithering signals, i.e. switch (A) goes to the scanning signal and switch (B) is open, to scan the wavelength of the laser over a single water vapour absorption line. After finding the absorption line we want, adjust

the offset of the phase-sensitive detector for the centre of the absorption line to be zero. Second, after turning off the scanning signal, find the suitable the dc level for the centre of the absorption line by means of the output of the phase-sensitive detector. Third, reset the integrating amplifier and turn on switch (B).

This wavelength locking circuit is a closed-loop circuit and the gain of the integrating circuit is not very important. However, if the gain of the integrating amplifier is too small or big, then this circuit can not reach a stable state. Therefore, this circuit and the current controller of the laser should be calibrated together.[33]

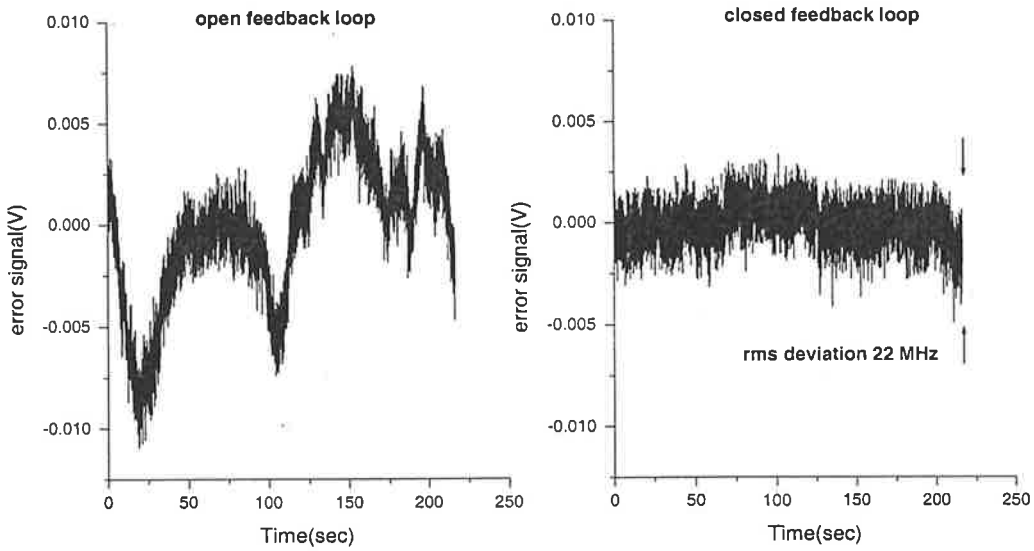

Figure 6.24 : Stability of the wavelength of the master laser from the centre of the water vapour absorption line, 832.04184 nm.

The zero point of the error signal voltage in Figure 6.24 represents the centre of the water vapour absorption line, 832.04184 nm. The relation between the error signal voltage of the phase-sensitive detector and the actual frequency of the laser was obtained by Fabry-Perot. When the error signal voltage increased 1 mV, then the peak of the output of Fabry-Perot moved 25MHz. In other word, 1mV of the error signal represents the 25MHz variation of the frequency of the laser. Using the injection current locking circuit in Appendix A and the external port of the current controller, the rms frequency deviation of the wavelength of the master laser from 832.04184 nm, the centre of the water vapour absorption line, is 22MHz as shown in Figure 6.24.

This satisfies the frequency stability requirement for water vapour detection in the atmosphere as shown in Table 2.1.

To achieve better stability of the wavelength of the laser using this method, more thermally stable electric component and more precise gain calibration of the circuit will be needed. In addition, we may improve the stability of the laser by adding a differential amplifier to the current locking circuit.[33]

Chapter 7

Experiment III

Telescopes for transmitting and receiving

This chapter is about the telescopes of our DIAL to transmit laser beam and to receive the scattered signal by aerosols and water vapour in the atmosphere. In addition, the experiment to measure the beam diameter and divergence of the transmitted beam is discussed.

In section 7.1, the receiving and transmitting telescopes and the mount for a single mode optical fibre and a photodiode are discussed. In section 7.2, the experiment to measure the beam diameter and divergence of the laser beam after the transmitting telescope is discussed. In section 7.3, the test of the telescopes, i.e. the transmitting and receiving telescopes, with a silicon photodiode is discussed.

7.1. The telescopes

The receiving telescope of our DIAL is a Schmitt-Cassegrain telescope (Celestron, G-8) and a brief diagram is shown in Figure 7.1 (A). The distance between the primary and the secondary mirrors of the receiving telescope can be adjusted so that the distance between the focal plane of the image and the rear part of the primary mirror can be adjusted.

Figure 7.1 (B) is a simplified diagram of the receiving part of our DIAL system. A single mode optical fibre is connected to the transmitting telescope - a Keplerian telescope - that is mounted on the place of the finder-scope of the receiving telescope. To mount a photodiode on the receiving telescope, we use a single lens reflex camera. This camera is installed in the place of the eyepiece holder of the receiving telescope. The photodiode is attached on the rear part of the camera as shown in Figure 7.1 (B).

The viewfinder of this camera can help us to focus the scattered light on the centre of the photodiode.

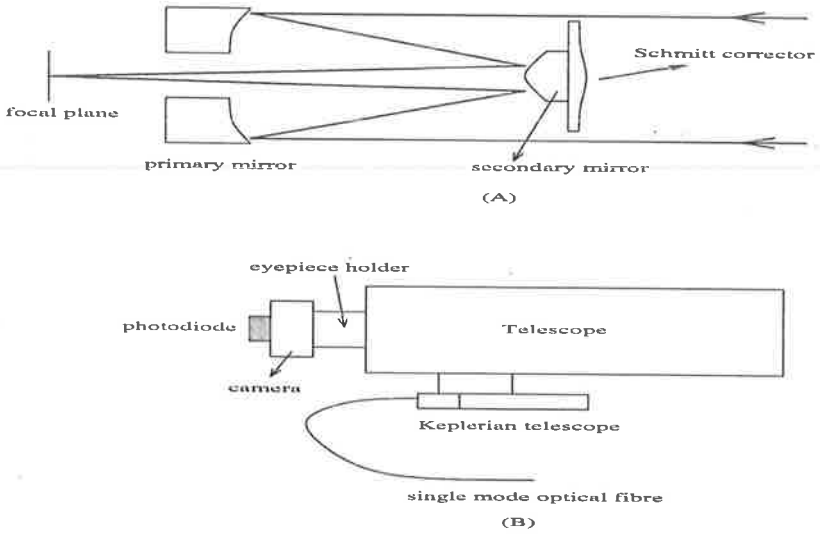

Figure 7.1 : Diagram of the receiving part

7.2. Beam diameter and divergence

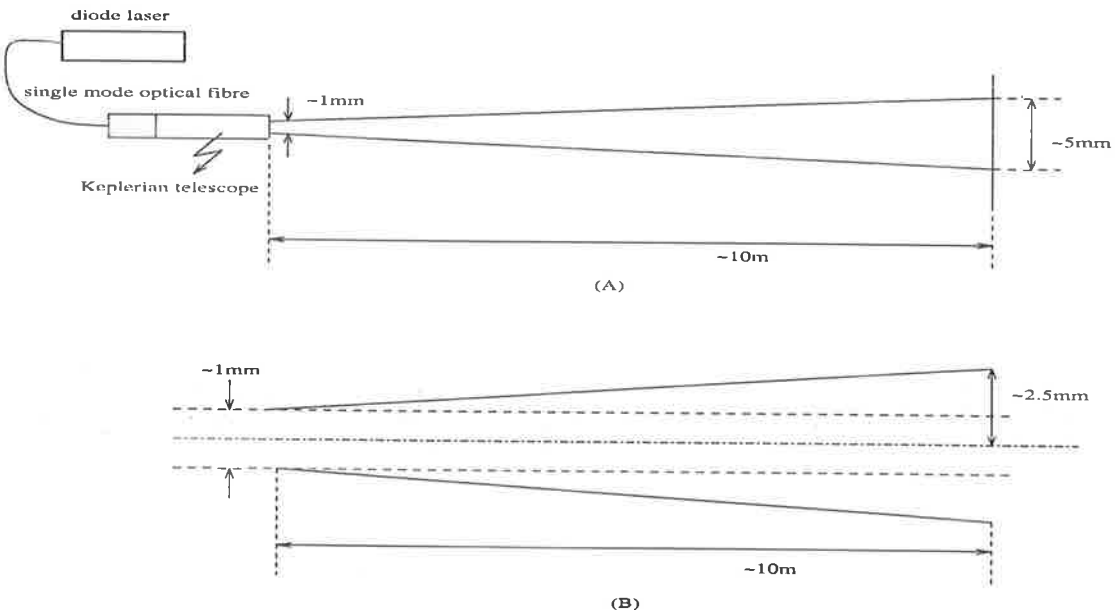

Figure 7.2: Schematic to measure the beam diameter and divergence of the laser beam after the transmitting telescope

The main reason to use a single mode optical fibre (3M, P1-4224-FC-10, diameter ≡ 5.5μm, Numerical Aperture ≡ 0.12) is that the divergence of laser beam should be small enough comparing to the field of view of the receiving telescope as the laser beam is transmitted into the atmosphere. Therefore, the transverse mode of the transmitted beam must be close to TEM_{00} mode and also the intensity profile shape should be circular.

The output of the optical fibre is collimated by a lens (Thorlabs, F220FC-B, f = 11mm) and the ratio between the input and the output power of this single mode optical fibre, i.e. the coupling power efficiency, is about 45%. Discussions about the coupling methods and the coupling lenses for single mode optical fibres can be found in Ref. 34.

The schematic to measure the beam diameter and divergence of the transmitted beam is shown in Figure 7.2. The distance between the transmitting telescope and screen is about 10m and the beam diameter in the screen is about 5mm. Using this value, we can calculate the divergence angle as below.

$$\tan(\theta) = \frac{0.0025 - 0.005}{10}$$
$$\therefore \ Divergence\,(2\theta) = 0.4 \ \text{(mrad)} \tag{7-1}$$

The divergence angle of the transmitted beam after the transmitting telescope is about 0.4 mrad and this satisfies the requirement of the laser for water vapour detection which is presented in Table 2.1.

7.3. Test of the telescopes with a silicon photodiode

The schematic of the test of the telescopes with a silicon photodiode (UDT-PIN 10DP) is shown in Figure 7.3. The laser beam is chopped by means of an Acousto-Optic Modulator (AOM) and the first order of the AOM is coupled with a single mode optical fibre. The distance between the transmitting telescope and the wall is about

75m. The output of the silicon photodiode is shown in Figure 7.4, when the pulse width of the transmitted beam is about 7 ms.

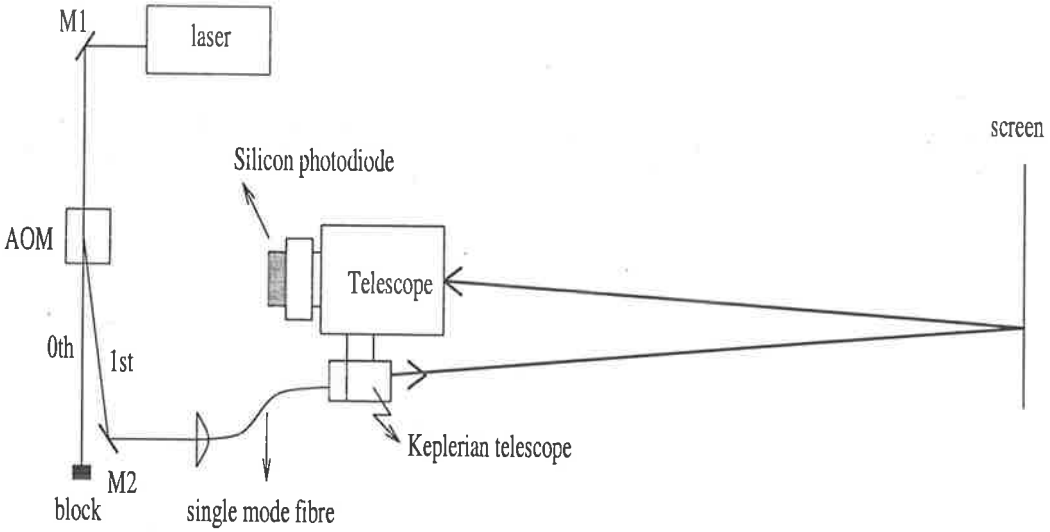

Figure 7.3 : Schematic of the test of the telescopes with a silicon photodiode

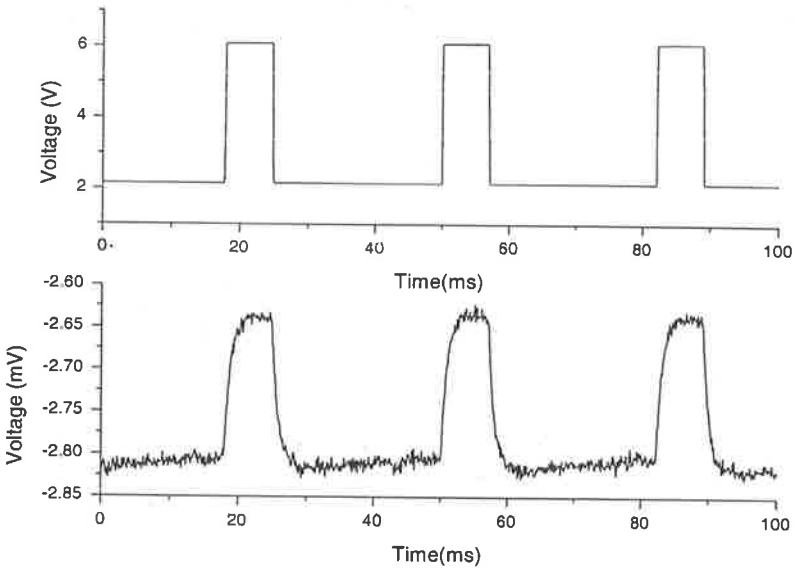

Figure 7.4 : The upper figure is the trigger output to the AOM and the lower is the output of the photodiode installed in the receiving telescope.

Chapter 8

Conclusions and future plans

Frequency modulation spectroscopy was done to investigate water vapour absorption lines with a free-running diode laser (Hitachi HG8325G) around 830nm and seven water vapour absorption lines were observed. This diode laser will be used as the master laser of our ground-based Differential Absorption Lidar (DIAL) system to profile the temporal and vertical distribution of water vapour in the lower atmosphere. A multi-pass absorption cell was constructed and 24m path length was achieved by means of 1.3m of the actual length of the cell. The wavelengths and the line strengths of the observed water vapour absorption lines were found as well comparing the frequency differences of the observed absorption lines with HITRAN database. The wavelength of the diode laser was scanned and modulated by the external port of either the current or the temperature controller. Using first harmonic detection, absolute humidity was measured and its value was compared with the value that was obtained by a hygrometer.

Using the output of a lock-in amplifier as the feedback signal to the current controller, the master laser of our DIAL system was locked to the centre of a water vapour absorption line, whose wavelength is 832.04184nm. The rms frequency deviation from the centre of the water vapour absorption line was 22MHz. This satisfies the frequency stability requirement for water vapour detection in the atmosphere.[17]

The transmitting telescope and the mount for a photodiode and a single mode optical fibre were built and installed on the receiving telescope of our DIAL system. The beam diameter and divergence after the transmitting telescope were measured. The divergence angle of the transmitted beam was 0.4 mrad, which satisfies the requirement of the laser for water vapour detection.[17] In addition, using a silicon photodiode and the master laser of the DIAL system that was chopped by a Acousto-Optic Modulator (AOM), the receiving part of our DIAL system was tested on a hard target.

8.1 Future plans

The power of the transmitter, i.e. laser, will be increased by an injection-locked master-slave design or a tapered amplifier. A photon counting circuit, a temperature controller, and the other electronics for an avalanche photodiode (APD) will be constructed. A data acquisitive system and metal housing for our ground-based DIAL will be needed as well. The data from our ground-based DIAL can be compared to that from the RADARs that were built by the Atmospheric group in the Department of Physics and Mathematical Physics of the University of Adelaide.

Appendix A
Injection-current locking circuit

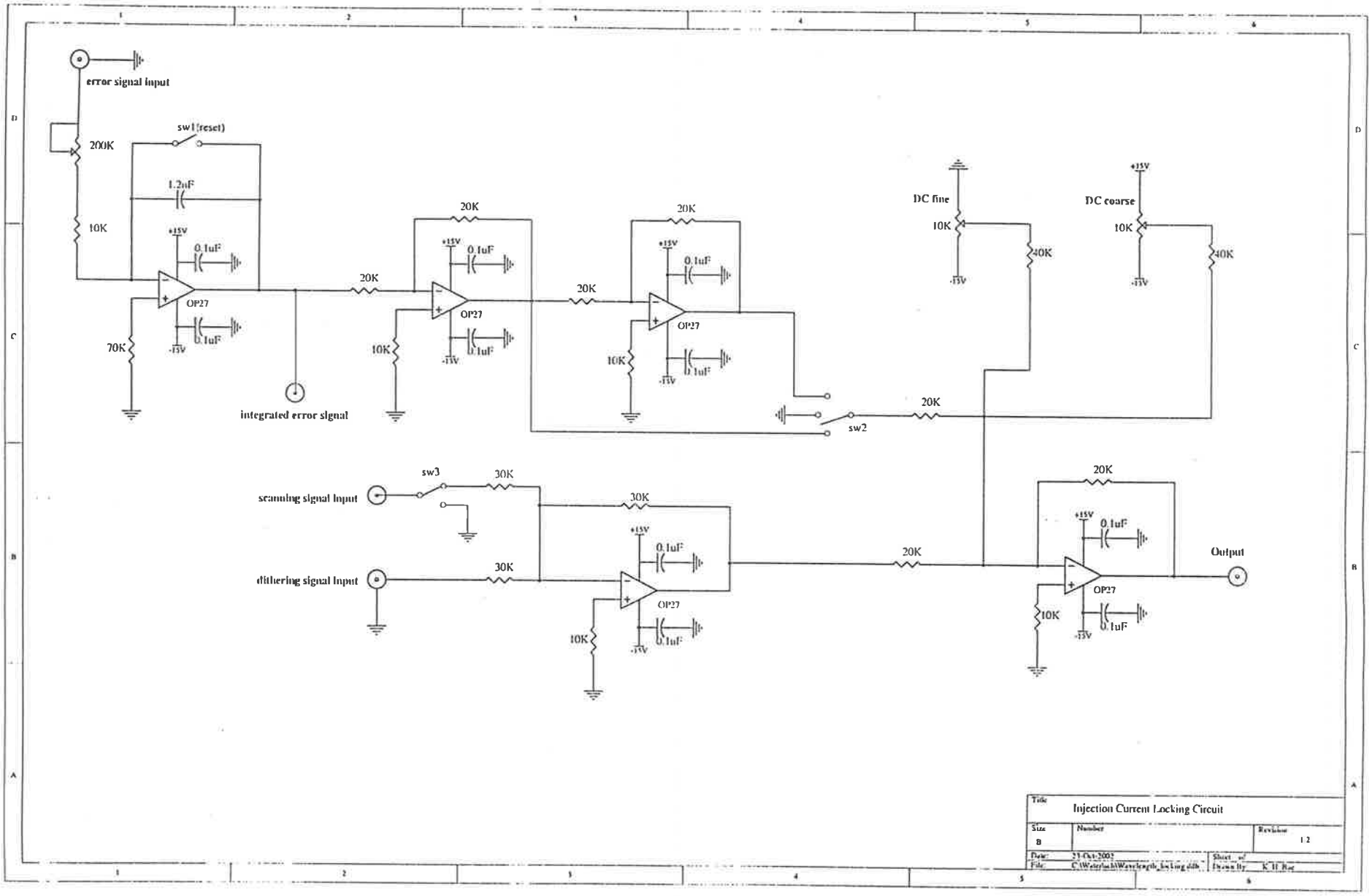
error signal input
sw1(reset)
200K
1.2nF
10K
+15V
0.1uF
OP27
-15V
70K
integrated error signal
20K
10K
sw2
DC fine
DC coarse
40K
sw3
30K
scanning signal input
dithering signal input
Output
Injection Current Locking Circuit
Size
B
Number
Revision
1.2
Date:
23-Oct-2003
Sheet of
File:
C:\Waterlock\Wavelength_locking.ddb
Drawn By:
K. H. Bae

Bibliography

1. R. M. Schotland, "Errors in the lidar measurements of atmosphere gases by differential absorption", J. Appl. Meteor., vol. 13, 71 (1974)
2. J. E. Harries, "Atmospheric radiation and atmospheric humidity", Quart. J. Roy. Meteor. Soc.,vol. 123, 2173- 2186 (1997)
3. European Space Agency, "WALES – WAter vapour Lidar Experiment in Space", (2001)
4. C. Werner and H, Herrmann, "Lidar measurements of the vertical absolute humidity distribution in the boundary layer", J. Appl. Meteorol., vol. 20, 476-481 (1981)
5. V. V. Zuev, V. E. Zuev, Y. S. Makushin, V. N. Marichev and A. A. Mitsel, "Laser sounding of atmospheric humidity: experiment", Appl. Opt., vol. 22, 3742 –3746 (1983)
6. E. R. Murray, R. D. Hake, J. E. Van der Laan, and J. G. Hawley, "Atmospheric water vapor measurement with a 10 micrometer DIAL system", Appl. Phys. Lett., vol. 28, 542-543 (1976)
7. P. W. Baker, "Atmospheric water vapor differential absorption measurements on vertical paths with a CO_2 lidar", Appl. Opt., vol. 22, 2257-2264 (1983)
8. R. M. Hardesty, "Coherent DIAL measurement of range-resolved water vapor concentration", Appl. Opt., vol. 23, 2545-2553 (1984)
9. W. B. Grant, J. S. Margolis, A. M. Brothers, and D. M. Tratt, "CO_2 DIAL measurements of water vapor", Appl. Opt., vol. 26, 3033-3042 (1987)
10. E. V. Browell, T. D. Wilkerson, and T. J. McIlrath, "Water vapor differential absorption lidar development and evaluation", Appl. Opt., vol. 18, 3474-3482 (1979)
11. C. Cahen, G. Mégie, and P. Flamant, "Lidar monitoring of the water vapor cycle in the troposphere", J. Appl. Meteorol., vol. 21, 1506-1515 (1982)
12. G. Ehret, C. Kiemle, W. Renger, and G. Simmet, "Airborne remote sensing of tropospheric water vapor with a near infrared differential absorption lidar system", Appl. Opt., vol. 32, 4534-4551 (1993)

13. D. Bruneau, H. Cazeneuve. C. Loth, and J. Pelon, "Double-pulse dual-wavelength alexandrite laser for atmospheric water vapor measurement", Appl. Opt., vol. 30, 3930-3937 (1991)
14. N. S. Higdon, E. V. Browell, P. Ponsardin, B. E. Grossmann, C. F. Butler, T. H. Chyba, M. N. Mayo, R. J. Allen, A. W. Heuser, W. B. Grant, S. Ismail, S. D. Mayor, and A. F. Carter, "Airborne differential absorption lidar system for measurements of atmospheric water vapor and aerosols", Appl. Opt., vol. 33, 6422-6438 (1994)
15. P. Ponsrdin, N. S. Higdon, B. E. Grossmann, and E. V. Browell, "Spectral control of an alexandrite laser for an airborne water-vapor differential absorption lidar system", Appl. Opt., vol. 33, 6439-6450 (1994)
16. D. Bruneau, T. A. des Lions, P. Quaglia, and J. Pelon, "Injection-seeded pulsed alexandrite laser for differential absorption lidar application", Appl. Opt. vol. 33, 3941-3950 (1994)
17. V. Wulfmeyer and J. Bösenberg, "Ground-based differential absorption lidar for water-vapor profiling: assessment of accuracy, resolution, and meteorological application., Appl. Opt., vol. 37, 3825-3844 (1998)
18. J. L. Machol, R. M. Hardesty, J. B. Abshire, M. A. Krainik, G. W. Switzer, D. M. Cornwell, and M. A. Randall, "Development of a miniature water vapor DIAL system", in Proceedings of Fourth International Symposium on Tropospheric Profiling: Needs and Technologies, Snowmass, Colorado, September 21-25, pp. 212-214 (1998)
19. R. A. Vincent, S. Dullaway, A. MacKinnon, I. M. Reid, F. Zink, P. T. May, and B. H. Johnson, "A VHF boundary layer radar: First results", Radio Sci., vol. 33, 845-860 (1998)
20. A. Yariv, "Optical Electronics ", Saunders College Publishing (1991)
21. H. Kressel, J. K. Butler, "Semiconductor lasers and Heterojunction LEDS', Academic Press (1977)
22. M. G. Littman, H. J. Metcalf, "Spectrally narrow pulsed dye laser without beam expander ", Appl. Opt., vol. 17, 2224 (1978)
23. D. Wandt, M. Laschek, A. Tünnermann, H. Welling, "Continuously tunable external-cavity diode laser with a double grating arrangement ", Optics Letters, vol. 20, 390 (1997)

24. Manual of 'Hitachi GaAlAs laser diode HL8325G' (2000)
25. A. E. Siegman, "An introduction to Lasers and Masers ", McGraw-Hill (1971)
26. A. G. Fox and T. Li, "Resonant mode in a maser interferometer ", Bell Syst. Tech. J., vol. 40, 453-488 (1961)
27. H. Kogelnik and T. Li, "Laser beams and Resonators", Appl. Opt., vol. 15, 1550-1567 (1966)
28. http://cfa-www.harvard.edu/hitran HITRAN database (1996)
29. L. S. Rothman et al, "HITRAN Molecular Spectroscopic Database and HAWK(HITRAN Atmospheric Workstation): 1996 Edition", Journal of Quantitative Spectroscopy and Radiative Transfer", vol. 60, 665-710 (1998)
30. P. S. Argall, "LIDAR studies of the middle atmosphere", PhD. Thesis, The University of Adelaide (1993)
31. http://aesd.larc.nasa.gov/gl/tutorial/lidar, LIDAR tutorial from NASA Laser System Branch (2001)
32. J. A. Silver, "Frequency-modulation spectroscopy for trace species detection: theory and comparison among experimental methods", Appl. Opt., vol. 31, 707-717 (1992)
33. D. Mitchell Carr, "PID control and controller tuning techniques", Eurotherm Controls Inc. http://www.eurotherm.com (1986)
34. I. Ladany, "Laser to single-mode fiber coupling in the laboratory", Appl. Opt., vol. 32, 3233-3236 (1993)
35. D. R. Herriot, H. Kogelnik, and R. Kompfner, "Off-axis paths in spherical mirror resonators", Appl. Opt., vol. 3, 523-526 (1964)
36. J. B. McManus, P. L. Kebabian, and M. S. Zahniser, "Astigmatic mirror multipass absorption cells for long-path-length spectroscopy", Appl. Opt., vol. 34, 3336-3348 (1995)
37. J. A. Silver and A. C. Stanton, "Optical interference fringe reduction in laser absorption experiments", Appl. Opt., vol. 27, 1914-1916 (1988)
38. G. J. Koch, A. L. Cook, C. M. Fitzgerald and A. N. Dharamsi, "Frequency stabilization of a diode laser to absorption lines of water vapor in the 944-nm wavelength region", Optical Engineering, vol. 40, 525-528 (2001)

39. O. Grohe, H. Gottschiling, H. Jennewein and T. Tschudi, "Frequency stabilization of a semiconductor laser using water-vapor absorption lines", Optical Engineering, vol. 40, 529-532 (2001)
40. T. Iguchi, "Modulation waveforms for second-harmonic detection with tunable diode lasers", Journal of Optical Society of America B, vol. 3, 419-423 (1986)
41. D. C. Hovde, J. T. Hodges, G. E. Scace and J. A. Silver, "Wavelength-modulation laser hygrometer for ultrasensitive detection of water vapor in semiconductor gases", Appl. Opt., vol. 40, 829-839 (2001)
42. Instruction manual, LWM-6500B, ILX Lightwave Co. (1994)
43. C. Young, "Calculation of the absorption coefficient for lines with combined Doppler and Lorentz broadening", J. Quant. Spectrosc. Radiat. Transfer., Vol.5, 549-552, (1965)
44. R. M. Goody, "Atmospheric radiation", Oxford University Press (1964)
45. K. Huang, " Statistical Mechanics", John Wiley & Sons (1987)